

POLITECNICO DI TORINO
Master's Degree in Biomedical Engineering



**Politecnico
di Torino**

Exploring human lower limb kinematics in walking:
overcoming challenges with minimal inertial sensor
configuration using a robotic modeling approach

Christian Tucci

Supervisors:
Prof. Ing. Andrea Cereatti
Dott. Ing. Marco Caruso

Academic Year 2024/2025

Abstract

Estimating lower limb joint kinematics is crucial for assessing movement disorders, optimizing rehabilitation, and monitoring sports performance. Traditional clinical setups require marker-based systems with at least three markers per segment. Wearable IMUs offer an alternative by placing sensors on proximal and distal segments but remain bulky, time-consuming, and costly. This highlights the potential of a minimal sensor configuration. Selecting instrumented segments requires careful consideration. Prioritizing the pelvis, representing center-of-mass dynamics, and the feet, as movement end-effectors, aligns with established methods for estimating spatio-temporal parameters in free-living conditions [1].

This thesis extends previous work on a biomechanical model that estimates joint angles using anthropometric measurements and pelvis/feet orientations and positions. That work addressed measurement errors by applying constraints and an optimization framework to fit segment data while limiting hip, knee, and ankle motion. The model employs the Denavit-Hartenberg convention for standardized joint definitions and ISB-recommended rotation sequences. The SQP optimization algorithm minimizes differences between model-derived and sensor data. This thesis aimed to refine the model using marker-based stereophotogrammetry (SP) data as a reference to evaluate the feasibility of estimating joint kinematics with minimal input. The improved model was tested on a healthy subject under different speeds and simulating toe walking and asymmetric steps (PoliTO dataset). After that, a validation was performed in more complex scenarios (Madrid dataset) featuring uneven terrains: flat, zigzag, sponge-like, and irregular surfaces, also assessed on a mechanized tilting platform.

During model refinement, fixed anthropometric measurements introduced errors due to marker trajectory uncertainties and soft tissue artifacts. Frame-by-frame adaptation of segment lengths yielded Root Mean Square Error (RMSE) values of 1.9 deg, 4.2 deg, and 2.9 deg for hip, knee, and ankle respectively, comparing estimated joint angles with those from SP. Using fixed lengths resulted in additional errors of 1.8 deg, 3.2 deg, and 0.4 deg for the same joints. Moreover, joint angle plots exhibited saturation. RMSE values on the Madrid dataset were: 1.4 deg (1.3 deg) for right (left) hip, 5.0 deg (3.9 deg) for right (left) knee, 5.3 deg (6.2 deg) for right (left) ankle. Although limited differences were found across

terrains, the presence of slope slightly decreased accuracy (errors up 0.7 deg). Range of Motion (ROM) was computed as the difference between maximum and minimum joint angles over each gait cycle, then averaged across all cycles. A two-way ANOVA ($\alpha_i = 0.05$) revealed no significant influence of both terrain conditions and slope on ROM estimation ($p = 0.81$).

This study demonstrated the feasibility of a minimal configuration for gait kinematics estimation, with optimization compensating for measurement errors. Integrating anthropometric variability improved accuracy, though asymmetry and experimental uncertainties persist. Since the ultimate goal remains the use of fixed measurements, the next step will be modeling segment length uncertainty within the optimization to enhance robustness, supporting IMU-based applications.

Contents

Abstract	3
Acknowledgements	7
List of Tables	7
List of Figures	9
Acronyms	10
1 Introduction	11
1.1 Context and motivations	11
1.2 Challenge and aim of the thesis	12
1.3 Thesis outline	13
2 Theoretical background	14
2.1 Introduction to lower limb kinematics	14
2.2 Technologies available for joint kinematics estimation	18
2.3 Stereophotogrammetry and the Davis Protocol	21
3 Materials	22
3.1 PoliTO DATASET	22
3.1.1 Experimental setup PoliTO	23
3.1.2 Experimental protocol - PoliTO	25
3.2 Madrid DATASET	26
3.2.1 Testing conditions	26
3.2.2 Experimental setup - Madrid	29
3.2.3 Experimental protocol - Madrid	30
4 Methods	34
4.1 General description of the situation	34
4.2 Overview of the KINEMI model	34
4.3 Lower limb model	35
4.3.1 The Denavit - Hartenberg convention	35
4.3.2 The developed input model	38
4.4 SP - based information	40

4.4.1	Data pre - processing	42
4.5	Optimization cycle	46
4.5.1	The Sequential Quadratic Programming (SQP)	47
4.5.2	Objective Function	49
4.6	Joint Angles and positions	51
4.7	Data analysis	51
4.7.1	Root Mean Square Error (RMSE) and Range of Motion (ROM)	51
4.7.2	Statistical analysis	52
5	Results	55
5.1	Dataset - Turin	56
5.2	Dataset - Madrid	57
5.3	Effect of walking condition on model estimation	59
6	Discussion	60
7	Conclusions	63
	Bibliography	64

List of Tables

1	Demographic and anthropometric details of the subjects used for model validation. The table includes information on gender, height, and weight for each participant.	26
2	DH parameters for the pelvis	39
3	DH parameters for the lower limbs	39
4	Minimum input model.	50
5	This table shows the RMSE values for each condition of walking (dynamic**), with values presented for each joint (RHip, RKnee, RAnkle, LHip, LKnee, LAnkle). The data include the mean RMSE values.	56
6	Condition Averaging: This table shows the RMSE values for each subject, with values presented for each joint (RHip, RKnee, RAnkle, LHip, LKnee, LAnkle). The data include the mean RMSE values, as well as the 25 th and 75 th percentiles for each joint across the subjects.	57
7	(Subject Averaging): This table presents the RMSE values averaged across subjects for each condition. The values are organized by joint (RHip, RKnee, RAnkle, LHip, LKnee, LAnkle), showing the mean RMSE for each joint across the different conditions.	58
8	This table presents the ROM values averaged across subjects for each condition, along with the observed absolute errors. The values are organized by joint (RHip, RKnee, RAnkle).	58
9	This table presents the ROM values averaged across subjects for each condition, along with the observed absolute errors. The values are organized by joint (LHip, LKnee, LAnkle).	59
10	This table presents p-values from the two-way ANOVA test for each factor considered.	59

List of Figures

1	Illustration of the pelvic coordinate system (XYZ), femoral coordinate system (xyz) and the JCS for the right hip joint [2].	15
---	--	----

2	The knee joint coordinate system as defined by Grood and Suntay [3].	16
3	Illustration of the JCS for the right ankle joint complex [2].	17
4	Typical gait ranges of motion for the hip, knee and ankle. Adapted from [4].	18
5	Components of a stereophotogrammetric system	19
6	Application example of a markerless motion capture system. Taken from [5]	20
7	On the left the PolitoBIOMed Lab, on the right the active wand.	24
8	Front view of marker placement on the subject [6].	24
9	Rear view of marker placement on the subject [6].	25
10	Condition 0 - flat surface.	27
11	Condition 2 - M.	28
12	Condition 3 - MAT.	28
13	Condition 4 - Terrasensa.	28
14	Overview of the 4 different terrains, also applied on the tilting platform.	29
15	on the left the LosMadronos - MotionAnalysis Lab, on the right the tilting platform.	30
16	Example of how the structure "data.mat" is nested	32
17	Example of how the structure "data.mat" is nested	33
18	Sagittal view of the diagram representing the situation under analysis.	34
19	Overview of the KINEMI model	35
20	Frontal and sagittal views of the human lower limb model, developed according to the DH convention and ISB guidelines. Joint numbering ranges from 1 to 3 for the pelvis and from 1 to 9 for each lower limb. Links depicted as thin blue lines indicate segments with zero length. Taken from [7].	36
21	Denavit-Hartenberg convention [8].	37
22	Overview of the KINEMI model, explicitly detailing the quantities obtained from the lower limb model.	40
23	Representation of the lower limb skeletal structure with highlighted joint centers [6].	41
24	Overview of the KINEMI model, explicitly detailing the quantities obtained from the SP.	42

25	Example of the HIP structure in which both rotation matrices and joint angles are stored. The same applies to KNEE and ANKLE.	43
26	Overview of the first alignment step.	44
27	Overview of the second alignment step.	45
28	The rotation from the local SR of the pelvis into the corresponding base SR is shown here. The same is done for the femur, tibia and foot segments following the rotations explained above.	46
29	General schematic representation of the basic SQP algorithm [9]. The functions $f(x)$, $h(x)$, and $g(x)$ can be nonlinear, with x potentially representing a vector of multiple optimization variables. In this case, $h(x)$ and $g(x)$ correspond to systems of equations. The term ∇_{xx}^2 denotes the Hessian matrix.	48
30	Objective function for the SQP algorithm.	49
31	Computation of the difference between the observed rotation matrix and that estimated by the model, with subsequent conversion to Euler Angles. Note that the symbol “ \times ” denotes standard matrix multiplication, not the cross product.	49
32	Optimization process made explicit	51
33	Left and right limb angles for hip, knee and ankle from the model (in blue) and SP (in red) - flat condition	55
34	Left and right limb angles for hip, knee and ankle from the model (in blue) and SP (in red) - terrasensa condition	56

Acronyms

AJC Ankle Joint Center

ANOVA Analysis of Variance

DH Denavit - Hartenberg

DoF Degree of Freedom

GRS Global Reference System

IMU Inertial Measurement Unit

ISB International Society of Biomechanics

JCS Joint Coordinate System

KINEMI Kinematics With Minimum Input

K-S Kolmogorov - Smirnov

QP Quadratic Programming

RMSE Root Mean Square Error

ROM Range Of Movement

SP Stereophotogrammetry

SQP Quadratic Programming

SR Reference System

1 Introduction

1.1 Context and motivations

Understanding human movement through the analysis of joint kinematics plays a key role in the quantitative assessment of joint behavior in terms of position, angle and velocity. “A complete understanding of joint kinematics is important in the diagnosis of joint disorders resulting from injury or disease, in the quantitative assessment of treatment, in the design of better prosthetic devices, and in the general study of locomotion” [3]. Quantitative instrumental gait analysis provides clinicians with accurate and reliable data that are valuable for diagnosing motor disorders, planning surgical interventions and designing prosthetic devices [10]. In rehabilitation, it enables the assessment of functional limb performance under normal and abnormal conditions, guiding treatment strategies and monitoring progress. For example, patients with Parkinson’s disease often present with specific gait abnormalities, such as reduced stride width and altered joint orientation, which may be difficult to detect with traditional clinical assessments alone [11].

Despite its clinical potential, the integration of advanced kinematic analysis methodologies into routine practice remains limited by logistical and technical barriers. Current approaches are predominantly confined to controlled environments, such as clinics or laboratories, which restrict their ability to capture comprehensive movement patterns representative of daily life. Future advancements aim to extend kinematic analysis capabilities to real-world settings, bridging the gap between laboratory conditions and natural environments. Emerging technologies, such as inertial measurement units (IMUs), offer promising solutions that are portable, cost-effective, and non-invasive. These innovations could enable continuous gait monitoring in real-life conditions [12].

In rehabilitation, quantifying joint kinematics during therapy sessions provides valuable information on therapy dosage, which is closely linked to recovery outcomes. For instance, in stroke rehabilitation, the extent of joint motion during therapy has been shown to correlate with improvements in gait speed [13]. Such data facilitate the development of personalized rehabilitation plans and allow for the ongoing adjustment of therapy strategies based on objective evidence.

While current efforts focus primarily on clinical applications, joint kinematics analysis has the potential to reshape the monitoring and understanding of motor

health. By enabling precise, data-driven assessments, this field enhances patient care and provides a foundation for broader applications in the future.

1.2 Challenge and aim of the thesis

This thesis builds upon the preliminary work conducted in a previous study [7], which addressed the challenges of reducing the number of sensors required for estimating lower limb kinematics in real-world applications. The prior work focused on validating a minimal sensor configuration using three inertial measurement units (IMUs), two on the feet and one on the pelvis, to estimate spatio-temporal parameters [1]. While this configuration provided several advantages, such as lower costs, improved wearability, and reduced preparation time, it also introduced significant challenges.

Specifically, although the reduced dataset theoretically allows for a unique estimation of knee kinematics from a mathematical perspective, additional constraints were introduced. Furthermore, the validation was conducted under controlled in-lab walking conditions to ensure consistency and reliability in the results.

That said, this thesis work takes a step back to investigate data derived from stereophotogrammetry (SP), acquired using the Davis protocol, to assess the feasibility of a future integration with IMUs, highlighting the limitations of this approach. The stereophotogrammetry-based dataset, includes the position and orientation of the pelvis, knees, ankles, and feet. The dataset includes the position and orientation of the pelvis, knees, ankles and feet. However, the developed *minimum input model* relies only on the position and orientation of the pelvis and feet to estimate lower limb kinematics mathematically. Despite the reduced input, the system remains mathematically determined, ensuring a unique solution for the kinematics estimation. The model is first built and tested on a healthy subject under simulated and controlled normal walking conditions. It is then tested and validated on a dataset of healthy subjects under walking conditions on different uneven terrains. This made it possible to overcome the constraints of flat and controlled laboratory environments. The inclusion of irregular terrain broadens the applicability of the method, with the ultimate goal being to integrate its use with IMUs.

1.3 Thesis outline

The thesis is structured as follows:

- **Chapter 1** introduces the context and motivation for the research, highlights the challenges and outlines the aims of the thesis itself.
- **Chapter 2** provides a theoretical background, discussing the fundamentals of lower limb kinematics, existing technologies for joint kinematic estimation, and a detailed overview of stereophotogrammetry.
- **Chapter 3** details the materials used in the study. The experimental protocol and setup, the instrumentation and the datasets employed are detailed.
- **Chapter 4** details the methods used in the study, from the optimization framework (cambio) to the statistical analysis.
- **Chapter 5** the results obtained with the implemented optimization framework (cambio) are displayed.
- **Chapter 6** the results presented in Chapter 5, the limitations and the potential improvements are critically discussed.
- **Chapter 7** summarizes the work performed, discusses its impact on future research, and explores prospects for integrating inertial sensors and other potential applications.

2 Theoretical background

2.1 Introduction to lower limb kinematics

Joint kinematics is the quantitative description of the relative motion between two rigid, adjacent body segments, typically represented by bones. “The motions which occur in most anatomical joints involve three-dimensional movement which is described by six independent coordinates or degrees of freedom. Three are translations and three are rotations” [3].

The focus of this thesis is on the kinematics of the lower limbs, specifically analyzing the relative motion of adjacent segments (pelvis, thigh, shank, and foot) during walking. The motion of the main joints (hip, knee, and ankle) is characterized using joint angles defined according to international standards. In detail, the International Society of Biomechanics (ISB) standardized the Joint Coordinate System (JCS) proposed by Grood and Suntay for joint motion, defining rotation sequences and reference axes for the lower limb joints (hip, knee, and ankle) as follows below [3][2].

Hip joint

The hip joint angle represents the relative motion between the pelvis and femur, defined by flexion/extension, abduction/adduction, and internal/external rotation. Flexion/extension occurs in the sagittal plane around the mediolateral axis, abduction/adduction in the frontal plane around the anteroposterior axis, and internal/external rotation in the transverse plane around the vertical axis.

More specifically, the JCS is defined as follows:

1. **Origin:** at the center of the femoral head
2. **e1:** the axis fixed to the pelvis, parallel to the line connecting the left and right anterior superior iliac spines (ASIS), pointing to the right
3. **e3:** the axis fixed to the femur, along the long axis of the femur, pointing proximally
4. **e2:** the floating axis, perpendicular to both e1 and e3

The recommended rotation sequence for the hip joint is:

1. Flexion/extension around the e1 axis

2. Ab/adduction around the e_2 axis
3. Internal/external rotation around the e_3 axis

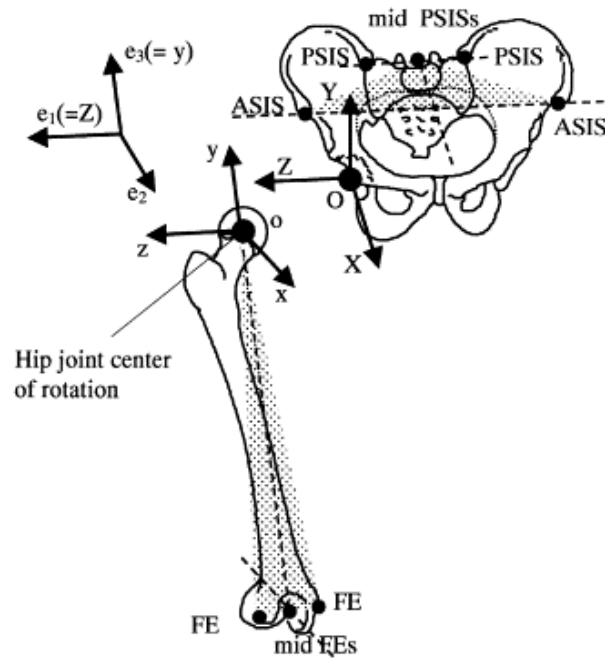


Figure 1: Illustration of the pelvic coordinate system (XYZ), femoral coordinate system (xyz) and the JCS for the right hip joint [2].

Knee joint

The knee is primarily a hinge joint, with flexion/extension as the main movement in the sagittal plane. Minor internal/external rotation and abduction/adduction may occur during complex movements or under significant loads.

Although not explicitly defined in Wu et al. (2002), the knee joint is typically described using a similar JCS approach:

1. **Origin:** at the midpoint between the femoral epicondyles
2. **e1:** the axis fixed to the femur, approximately parallel to the femoral epicondylar axis, pointing to the right
3. **e3:** the axis fixed to the tibia, along its long axis, pointing proximally

4. e_2 : the floating axis, perpendicular to both e_1 and e_3

The rotation sequence for the knee follows that of the hip joint.

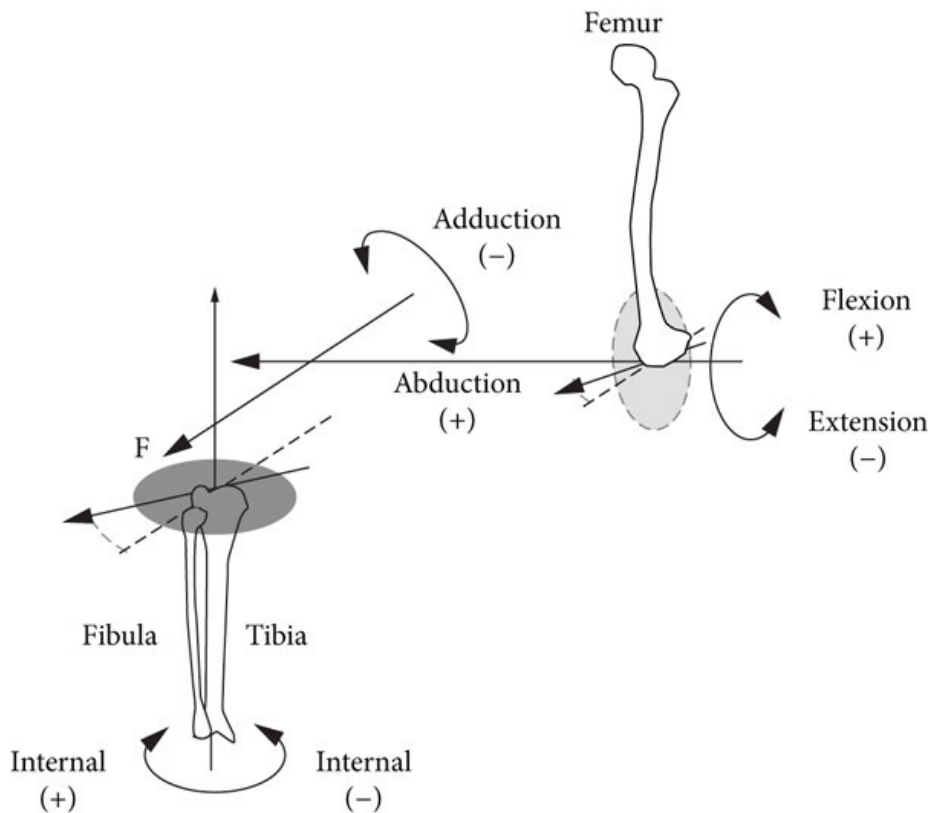


Figure 2: The knee joint coordinate system as defined by Grood and Suntay [3].

Ankle joint

The ankle comprises the talocrural and subtalar joints. Its primary motion, dorsiflexion/plantarflexion, occurs in the sagittal plane around the mediolateral axis. Limited inversion/eversion in the frontal plane and internal/external rotation also occur.

Specifically, the JCS is defined as follows:

1. **Origin:** at the midpoint between the malleoli
2. e_1 : the axis fixed to the tibia, passing through the malleoli, pointing to

the right

3. **e2**: the axis fixed to the foot, perpendicular to e1 and the plantar surface of the foot, pointing anteriorly
4. **e3**: the floating axis, perpendicular to e1 and e2

The recommended rotation sequence for the ankle joint is:

1. Dorsi/plantarflexion around the e1 axis
2. Inversion/eversion around the e2 axis
3. Internal/external rotation around the e3 axis

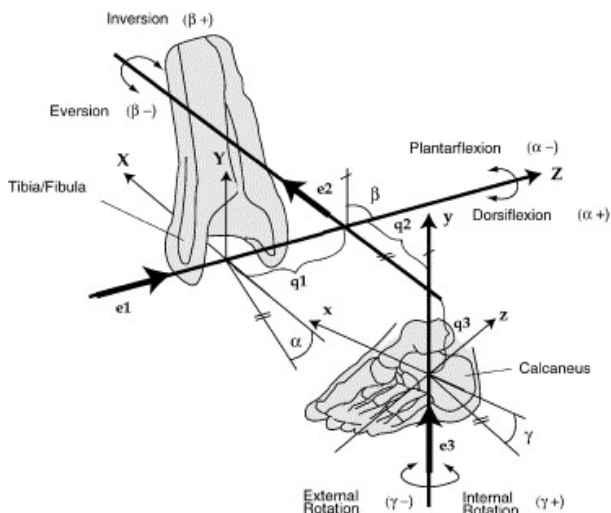


Figure 3: Illustration of the JCS for the right ankle joint complex [2].

In typical gait, the following ranges of motion are observed for the main joints:

- **Hip**: approximately 40° of flexion/extension, 10° of ab/adduction, and 15° of internal/external rotation. These movements are essential for leg advancement and maintaining balance.
- **Knee**: approximately 60° of flexion/extension. Knee motion is critical for shock absorption during the stance phase and for foot clearance during the swing phase.

- **Ankle:** approximately 30° of dorsiflexion/plantarflexion. Ankle motion ensures proper foot placement and propulsion during gait.

These ranges, shown graphically in Figure 4, may vary when walking on uneven terrain or engaging in activities such as running, climbing, or navigating slopes, where increased flexibility is needed to accommodate specific movement demands.

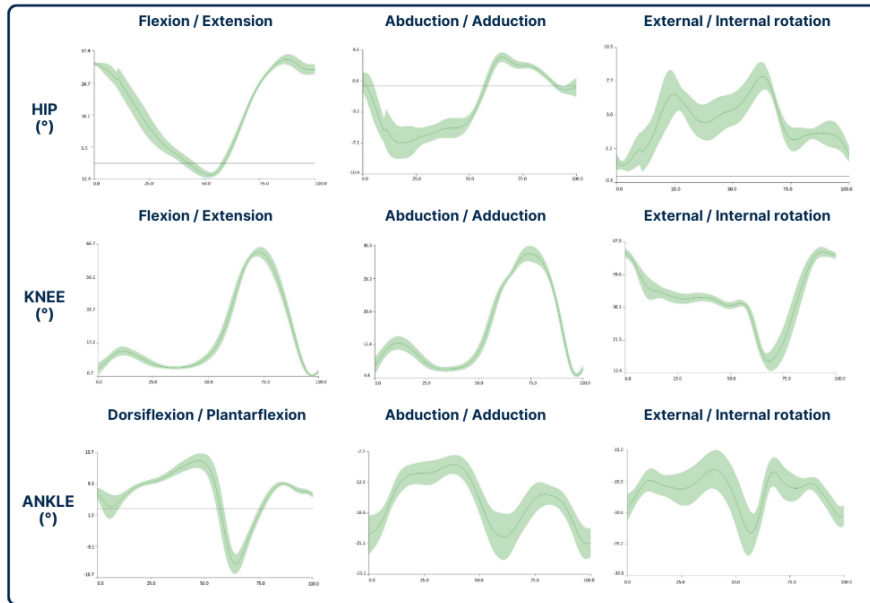


Figure 4: Typical gait ranges of motion for the hip, knee and ankle. Adapted from [4].

2.2 Technologies available for joint kinematics estimation

There are many technologies currently available for the study of joint kinematics, including both traditional methods and more innovative solutions [14][15]. However, the main operational and widely used technologies are described below: stereophotogrammetric (SP) systems, inertial measurement units (IMUs) and markerless systems.

1. Stereophotogrammetry (SP)

Stereophotogrammetry is an accepted technique for analyzing human movement, recognized as the gold standard in biomechanics. This methodology uses multiple cameras (the number depends on the case) strategically positioned around an acquisition volume to track reflective markers applied to specific anatomical points.

- **Advantages:** provides highly accurate and reliable data, ideal for applications in controlled and clinical environments.
- **Limitations:** requires a controlled environment, is expensive and is highly dependent on the correct placement and calibration of markers.

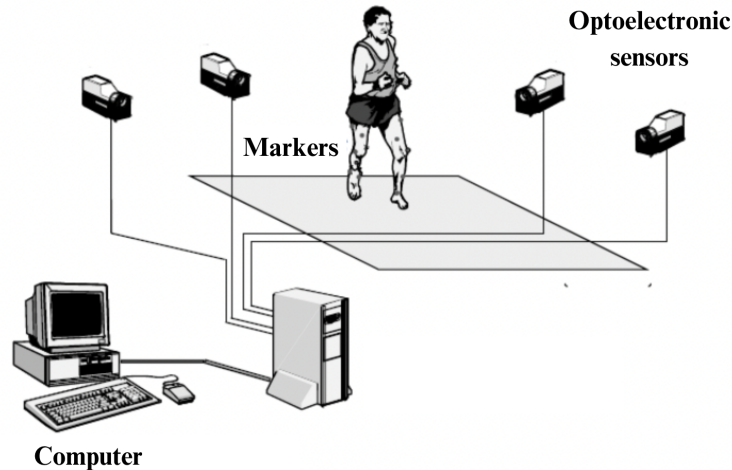


Figure 5: Components of a stereophotogrammetric system

2. Inertial measurement units (IMUs)

IMUs are wearable devices consisting of accelerometers, gyroscopes and, in some cases, magnetometers. These sensors work together to measure linear accelerations, angular velocities and orientations, enabling 3D motion tracking.

- **Advantages:** compact, inexpensive and capable of acquiring motion data in natural, unconstrained environments.
- **Limitations:** sensitive to drift errors, particularly during prolonged measurements, and require advanced algorithms for data processing

and error correction.

3. Markerless motion capture systems

Markerless systems utilize computer vision and machine learning techniques to estimate joint kinematics directly from video data. These systems analyze the movement of anatomical landmarks without the need for reflective markers, offering an accessible and non-invasive solution.

- **Advantages:** eliminates the need for markers, reducing setup time and complexity, and allows for motion tracking in outdoor or unconstrained environments.
- **Limitations:** typically less accurate than marker-based methods, with performance dependent on the quality of cameras and environmental conditions.

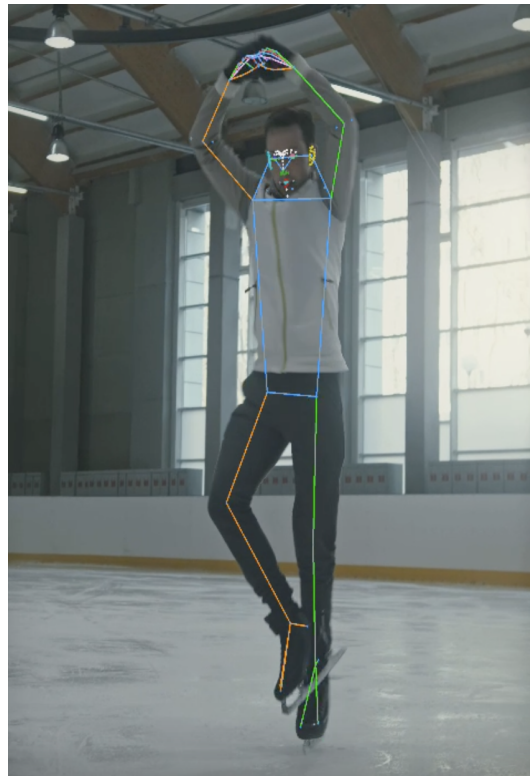


Figure 6: Application example of a markerless motion capture system. Taken from [5]

2.3 Stereophotogrammetry and the Davis Protocol

The technology used in this thesis is therefore stereophotogrammetry [see previous paragraph]. Among the different protocols, this study used the Davis protocol, developed by Roy Davis et al. in 1991, which is used to place markers on subjects and calculate kinematic gait parameters [16]. It involves placing markers on specific anatomical points, as shown in Figures 15-16 for the lower body, to ensure repeatability and standardization of measurements. It assumes a rigid body model with pre-defined anthropometric parameters and requires specific calibration steps to estimate lower limb joint kinematics.

The key steps are as follows:

1. **Marker placement:** reflective markers are positioned according to Figures 15-16. These markers act as reference points for tracking segmental motion during dynamic trials.
2. **Calibration trials (static):** a static trial is conducted to estimate joint center locations relative to marker clusters. This step establishes the segment coordinate systems and defines the spatial relationship between markers and the underlying skeletal structure. These relationships are crucial for accurately mapping the marker trajectories to joint motion.
3. **Dynamic trials:** during movement, the relative motion of markers is recorded and processed to estimate joint kinematics. Using inverse kinematics, segmental rotations are calculated and decomposed into anatomical planes (sagittal, coronal, transverse) to estimate clinically relevant joint angles.

While the Davis Protocol provides robust estimates of lower limb kinematics, its accuracy is affected by factors such as marker misplacement, skin motion artifacts, and assumptions about rigid body behavior.

3 Materials

This chapter describes the materials, experimental setups and protocols used. The study uses a Vicon stereophotogrammetric system, adopting the PlugIn Gait protocol, which is an implementation of the Davis protocol, as described in Section 2.3.

The experimental setup included both optoelectronic markers and inertial measurement units (IMUs) for motion capture. However, it is important to note that only data derived from the optoelectronic markers were utilized for the analysis presented in this work. The inclusion of IMUs ensured a comprehensive dataset, which may be considered for future studies.

The stereophotogrammetric system was prepared through masking, full calibration, and the establishment of the laboratory reference frame prior to subject preparation. The subject was equipped with optoelectronic markers and IMUs for the walking trials. Static trials were recorded to facilitate manual labeling of markers, ensuring precise correspondence with camera-detected points. Post-processing was conducted using Nexus software, which included gap filling to address marker occlusions, execution of the dynamic pipeline, and data export in ASCII format for further analysis.

3.1 PoliTO DATASET

The dataset used for model development was sourced from [7], which reports motion capture data collected from a healthy volunteer performing various exercises to analyze straight walking under different conditions:

- Walking at different speeds:
 - Comfortable speed
 - High speed
 - Low speed
- Half-step walking:
 - Right half-step
 - Left half-step
- Toe walking

- Walking with different step lengths:
 - Short step length
 - Long step length

3.1.1 Experimental setup PoliTO

Experiments were conducted in the PolitoBIOMed Lab, a facility equipped with specialized instrumentation for movement analysis tests, as shown in Fig. 13.

Two systems were employed:

- **SP** system, consisting of:
 - 12 Vicon infrared cameras were used to reduce artefacts caused by natural light, ensuring accurate tracking,
 - 3 RGB cameras recorded video footage of the experiments,
 - An active wand aided in system calibration, featuring known geometric marker configurations, represented in Fig 13
 - 16 passive markers, coated with retro reflective material, were placed on the subject according to the Vicon’s reference guide [6], as shown in Fig. 14-15,
 - Nexus software (v 2.12) was utilized for extracting files containing joint angles and forces.
- **IMU-based** system: a motion tracking system using seven IMUs was implemented, with the sensors attached to bands positioned on specific body segments, including the feet, shanks, thighs, and pelvis.



Figure 7: On the left the PolitoBIOMed Lab, on the right the active wand.

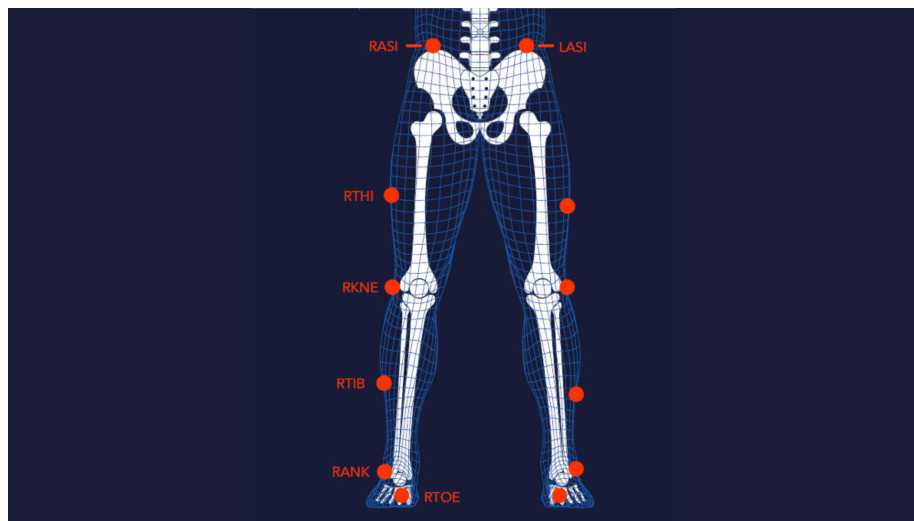


Figure 8: Front view of marker placement on the subject [6].

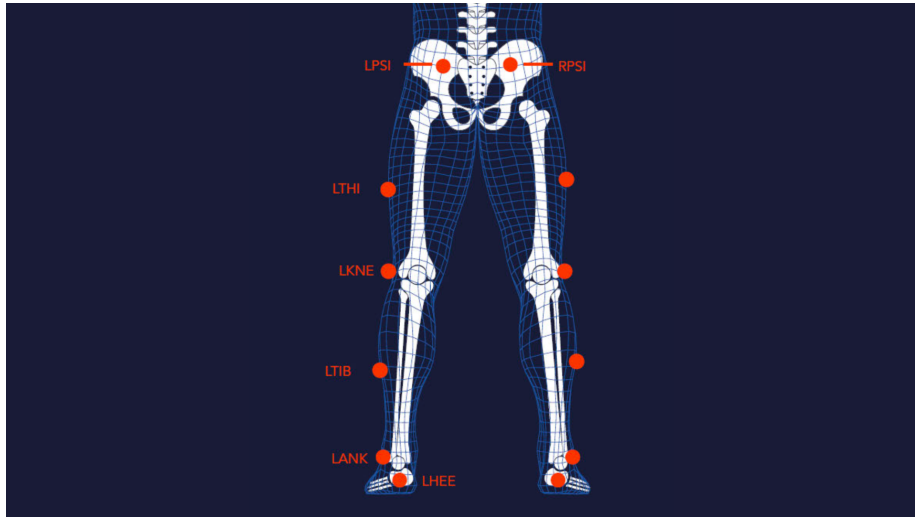


Figure 9: Rear view of marker placement on the subject [6].

3.1.2 Experimental protocol - PoliTO

Following the protocol established in [7], the exercises described in Section 3.2.1 were acquired and analyzed using the combined SP and IMU systems, as follows:

1. 10 minutes of warm-up of IMUs,
2. preliminary acquisition in static condition of one minute of the IMUs to estimate the bias of the gyroscope,
3. start acquisition with IMU software,
4. start recording with Nexus,
5. performance of the first exercise,
6. stop recording with Vicon,
7. stop IMUs' acquisition,
8. repeat the steps 3-7 until reaching at least 3 trials,
9. repeat the steps 3-8 for each exercise.

3.2 Madrid DATASET

The dataset used for model validation consists of gait recordings from five healthy adult subjects. The study adhered to all ethical guidelines and was approved under IRB code 218/2022. All participants provided informed consent prior to data collection. The demographic and anthropometric details of the participants are as follows:

Subject	Gender	Height (m)	Weight (kg)
Subject 1	F	1.66	51
Subject 2	F	1.67	52
Subject 3	M	1.87	87
Subject 4	F	1.76	72
Subject 5	M	1.85	85

Table 1: Demographic and anthropometric details of the subjects used for model validation. The table includes information on gender, height, and weight for each participant.

These subjects represent a diverse range of body types, enhancing the model’s robustness when tested under different biomechanical conditions.

The dataset includes static and dynamic trials:

- **Static trials:** used for calibration to establish baseline anatomical models and joint center positions.
- **Dynamic trials:** recorded during walking at a self-selected comfortable speed.

3.2.1 Testing conditions

In this study, subjects were recorded walking under various surface and slope conditions. The experimental protocol involved the following surface types:

- **Flat surface:** a standard, even surface designed to simulate typical walking conditions, with a uniform texture that provides consistent feedback underfoot. This surface serves as a baseline for comparison with more challenging terrains.

- **M:** the surface M is constructed using square modules, each measuring 500×500 mm, with an individual inclination angle of 15 degrees. A total of 13 such modules were used to create the zig-zag profile, alternating between peaks and valleys. This uneven terrain simulates conditions that require dynamic adjustments in gait and balance, as the foot transitions between raised and lowered sections.
- **MAT:** a soft and spongy surface, such as rubberized flooring or padded materials, which reduces the impact forces during walking. This surface simulates environments like gym floors or playgrounds, where cushioning might alter walking mechanics. The material has a density of 30 kg/m^3 .
- **Terrasensa:** an irregular surface featuring holes, varying roughness, and an assortment of obstacles that challenge the subject's proprioception and adaptability. This surface mimics natural outdoor terrains like forest paths or construction sites, where unevenness demands careful foot placement and dynamic adjustments to maintain stability. It is constructed using elements measuring $80 \times 500 \times 500$ mm, each weighing 3.5 kg.



Figure 10: Condition 0 - flat surface.



Figure 11: Condition 2 - M.



Figure 12: Condition 3 - MAT.



Figure 13: Condition 4 - Terrasensa.

Each surface condition was tested under two scenarios:

1. **No slope:** the surface remained horizontal, providing a neutral walking

plane.

2. **Slope:** the surfaces were placed on a mechanized tilting platform capable of inclinations up to 15 degrees, simulating uphill or downhill walking.

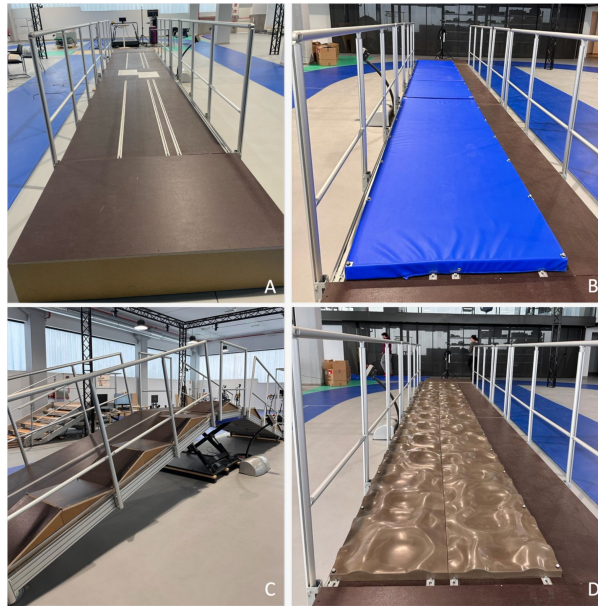


Figure 14: Overview of the 4 different terrains, also applied on the tilting platform.

3.2.2 Experimental setup - Madrid

The experiments were conducted in the Motion Analysis laboratory of Los Madronos Hospital, a facility equipped with specialized instrumentation for movement analysis tests as shown in Fig. 16.

As well as for the first dataset, two systems were employed:

- **SP** system, consisting of:
 - 12 Vicon infrared cameras were used to reduce artifacts caused by natural light, ensuring accurate tracking,
 - 2 RGB cameras (GoPro) recorded video footage of the experiments,
 - an active wand aided in system calibration, featuring known geometric marker configurations,

- 16 passive markers, coated with retro reflective material, were placed on the subject according to the Vicon’s reference guide [6], as shown in Fig. 14-15,
- the mechanically inclinable platform as shown in Fig. 16,
- 3 interchangeable removable platforms designed to simulate various terrain conditions, mounted onto the inclinable platform,
- Nexus software was utilized for extracting files containing joint angles and forces.



Figure 15: on the left the LosMadronos - MotionAnalysis Lab, on the right the tilting platform.

3.2.3 Experimental protocol - Madrid

The study involved five healthy subjects, as described in Section 3.2.2, whose walking was recorded under different ground conditions at a comfortable walking speed, according to testing conditions.

These conditions were meticulously captured and analyzed using the combined SP and IMU systems, as follows:

1. Configuration of the Vicon system, IMUs sensors,
2. two RGB cameras (GoPro) recorded video footage of the experiments,

3. execution of Vicon static and dynamic calibration, followed by IMUs calibration procedures,
4. all systems were synchronized, and data recording was initiated,
5. subjects performed the walking exercises under the specified conditions,
6. data acquisition was stopped after trial completion,
7. repeat the steps 3-6 until reaching 6 trials,
8. repeat the steps 3-8 for each condition.

After completing the acquisition procedure for both PoliTO and Madrid dataset, the data from the VICON system underwent processing to generate reference outputs. The standardization process resulted in the creation of the Matlab structures “data.mat”.

Specifically:

- The “*data.mat*” structure related to PoliTO dataset comprises multiple fields representing various trials. For each trial, data from different sensors are stored separately, as schematized in Fig. 17.

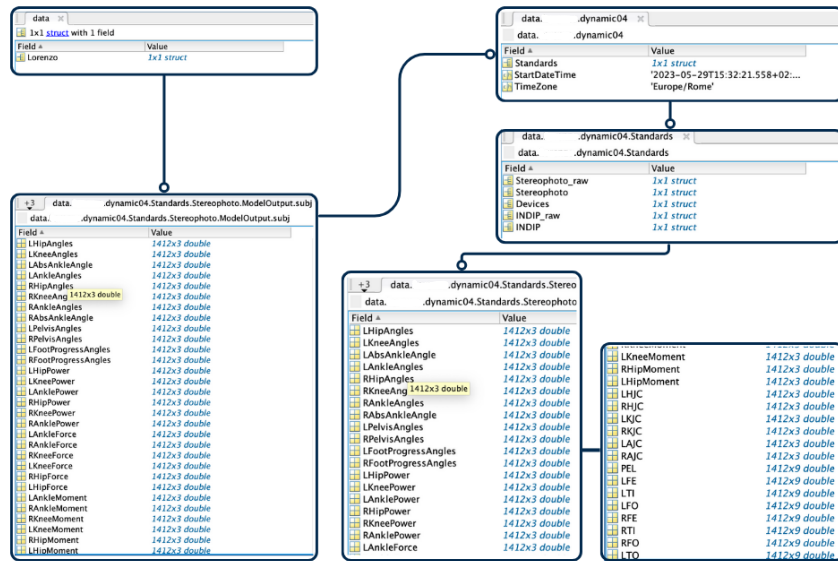


Figure 16: Example of how the structure "data.mat" is nested

- The "data.mat" structure related to Madrid dataset contains a field for each subject, each of which comprises 4 trials for each of the test conditions, as schematized in Fig. 18.

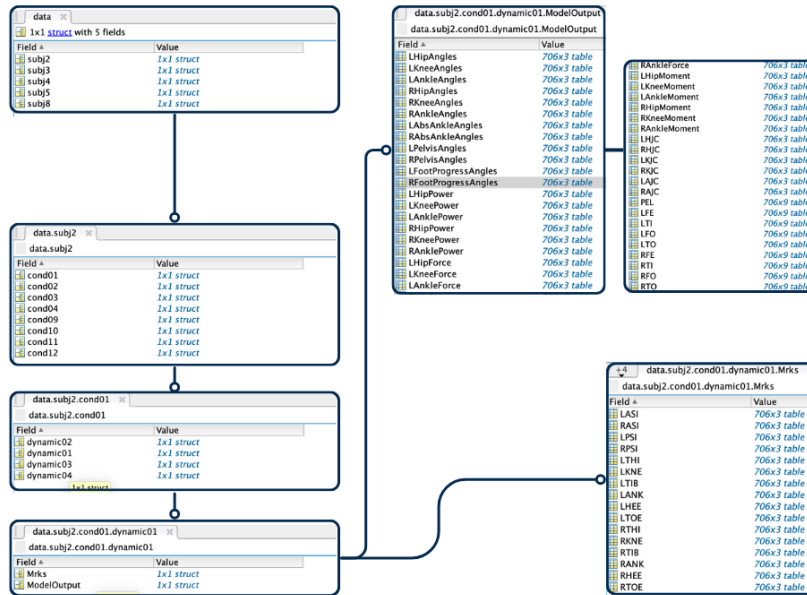


Figure 17: Example of how the structure "data.mat" is nested

4 Methods

4.1 General description of the situation

Figure 18 presents a sagittal perspective illustrating the context of the analysis. In particular, the process of estimating lower limb kinematics entails determining the joint angles at the hip, knee, and ankle, labeled as φ_1 , φ_4 , and φ_7 , respectively. “This is accomplished by leveraging the position and orientation information of the feet and pelvis, without possessing knee-specific information. The available data is incorporated into an optimization framework, aiming to reconstruct lower limb kinematics while adhering to established relationships among the three angles at the hip, knee, and ankle, connected by segments of known length.” [7].

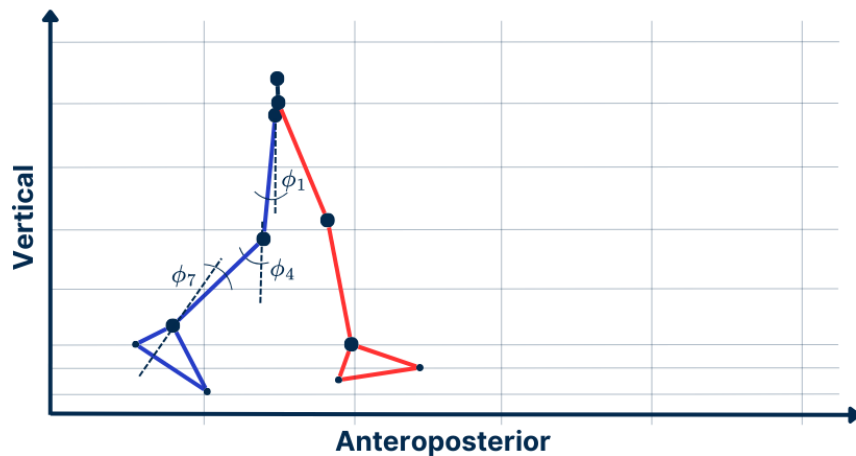


Figure 18: Sagittal view of the diagram representing the situation under analysis.

4.2 Overview of the KINEMI model

A model, named KINEMI (Kinematics with Minimum Input), was developed to estimate the kinematics of the lower limb by integrating anatomical modeling with stereophotogrammetric (SP) data, as shown in Figure 19. KINEMI model, implemented in MATLAB, consists of a central block that receives input from two sources: the lower limb model and the SP data. It then outputs the

angles and positions of the affected joints, enabling the reconstruction of joint kinematics (static and dynamic).

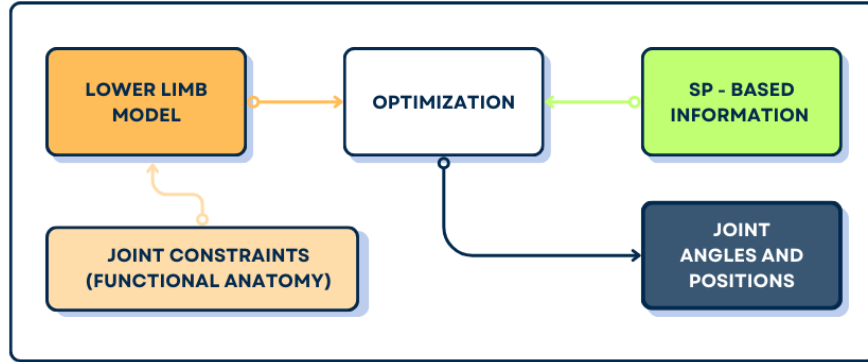


Figure 19: Overview of the KINEMI model

4.3 Lower limb model

4.3.1 The Denavit - Hartenberg convention

The initial input block for optimization involved the lower limb model, formulated as a kinematic chain based on the Denavit-Hartenberg (DH) convention, a systematic methodology used in robotics and kinematics to describe the spatial relationship between consecutive links in a robotic chain or kinematic structure [8]. A representation of the model is shown in Figure 20.

In the DH convention, each link and joint in a kinematic chain is represented using a coordinate frame. The relative position and orientation of one frame to the next are described using a 4x4 transformation matrix. This transformation matrix is constructed using four parameters: a_i , d_i , α_i , and θ_i , where i refers to the link or joint index.

- a_i (**link length**): the distance between z_{i-1} e z_i axes along the x_i axis. It represents the offset along the common normal (perpendicular axis between two consecutive z-axes).
- d_i (**link offset**): the displacement along the z_{i-1} axis from the origin of frame $i - 1$ to the intersection point with the x_i axis.

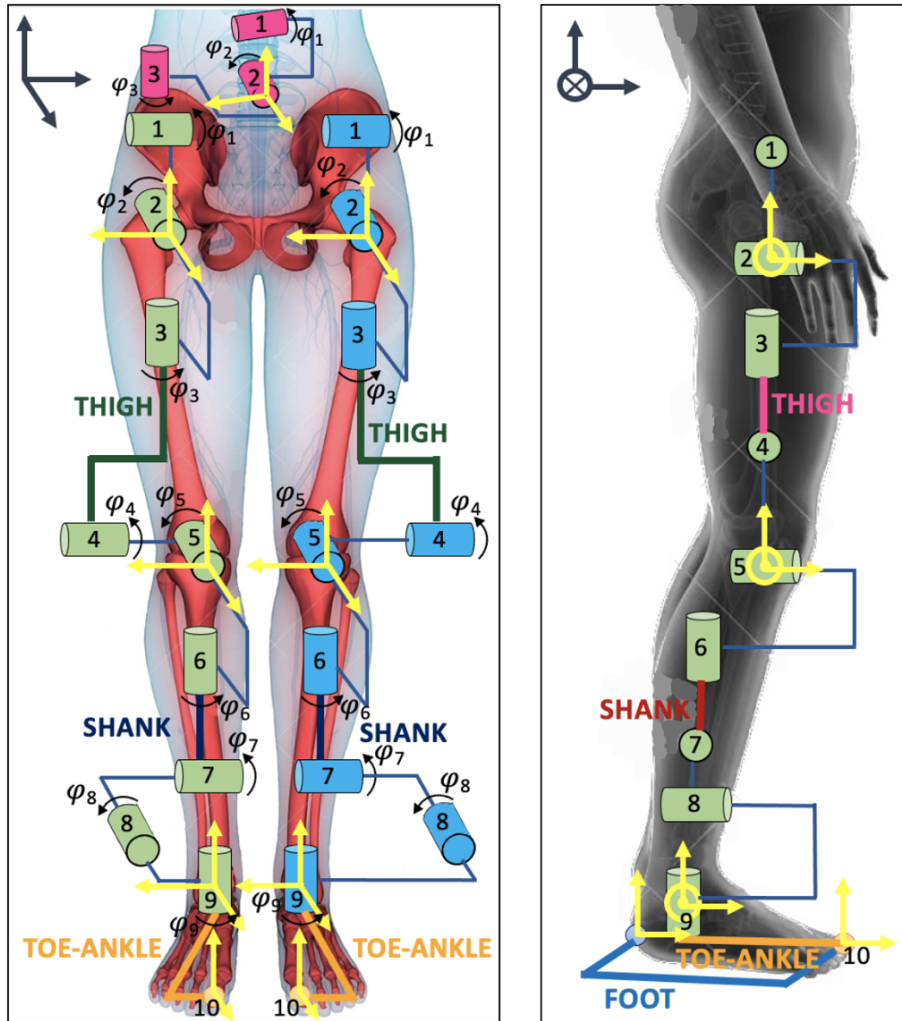


Figure 20: Frontal and sagittal views of the human lower limb model, developed according to the DH convention and ISB guidelines. Joint numbering ranges from 1 to 3 for the pelvis and from 1 to 9 for each lower limb. Links depicted as thin blue lines indicate segments with zero length. Taken from [7].

- α_i (**twist angle**): the angle of rotation between the z_{i-1} e z_i axes about the x_i axis. It defines the spatial orientation of the z-axes relative to one another.
- θ_i (**joint angle**): the angle of rotation between the x_{i-1} e x_i axes about the z_{i-1} axis. For revolute joints, θ_i is a variable, as it corresponds to the joint's rotational motion.

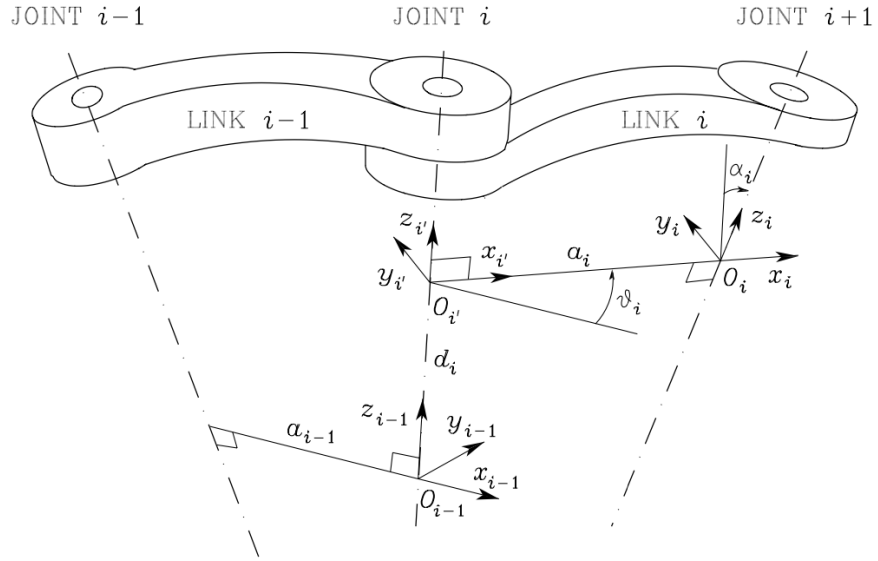


Figure 21: Denavit-Hartenberg convention [8].

According to the DH convention, each joint is represented with a single degree of freedom (DoF), where the rotation is described by φ . In the case of a revolute joint, three of the four parameters (a_i , d_i , and α_i) remain constant, as they are determined by the geometric relationship between consecutive joints defined by the i^{th} link. The only parameter that varies over time is θ_i [7].

The transformation matrix A_i^{i-1} describes the pose of frame i relative to frame $i-1$ and is constructed as:

$$A_i^{i-1} = \begin{bmatrix} \cos(\theta) & -\sin(\theta) \cos(\alpha) & \sin(\theta) \cos(\alpha) & a \cos(\alpha) \\ \sin(\theta) & \cos(\theta) \cos(\alpha) & -\cos(\theta) \sin(\alpha) & a \sin(\alpha) \\ 0 & \sin(\alpha) & \cos(\alpha) & d \\ 0 & 0 & 0 & 1 \end{bmatrix} \quad (1)$$

This matrix combines the effects of:

- Rotation about z_{i-1} by θ_i
- Translation along z_{i-1} by d_i
- Translation along x_i by a_i
- Rotation about x_i by α_i

The DH convention is mainly used for:

- **Forward kinematics:** calculating the end-effector's pose by multiplying transformation matrices for all links in the chain.
- **Inverse kinematics:** determining joint parameters for a desired end-effector pose.
- **Dynamic modeling:** simplifying motion equations for robotic manipulators.

While this convention provides a standardized and efficient framework for modeling and analyzing robotic kinematic chains, it can be tough to assign consistent frames in complex geometries and assumes idealized conditions that may not fully represent real-world systems.

4.3.2 The developed input model

In this thesis, the Denavit-Hartenberg convention is employed to represent the human lower limbs as a series of rigid links, incorporating the anthropometric lengths of each segment (l_{thigh} , l_{shank} , $l_{toeankle}$, l_{foot}).

The model incorporated 3 revolute joints for the pelvis and nine revolute joints for each lower limb. The joint definitions were established following the rotation sequences and axis orientations outlined by the ISB guidelines [2]. Each joint, including the pelvis, hip, knee, and ankle, was assigned three degrees of freedom (DoFs), covering flexion-extension, adduction-abduction, and internal-external rotation [17], as illustrated in Figure 20. Since all joints in the model are revolute, θ is the only parameter that depends on φ . The corresponding DH parameters used in this work are shown in Table 2 and Table 3.

Link	θ_i	d_i	a_i	α_i
1	$(\varphi_1 + \frac{\pi}{2})$	0	0	$\frac{\pi}{2}$
2	$(\varphi_2 + \frac{\pi}{2})$	0	0	$\frac{\pi}{2}$
3	$(\varphi_3 + \frac{\pi}{2})$	0	0	$\frac{\pi}{2}$

Table 2: DH parameters for the pelvis

Link	θ_i	d_i	a_i	α_i
1	$\varphi_1 + \frac{\pi}{2}$	0	0	$\frac{\pi}{2}$
2	$\varphi_2 + \frac{\pi}{2}$	0	0	$\frac{\pi}{2}$
3	$\varphi_3 + \frac{\pi}{2}$	$-l_{\text{thigh}}$	0	$\frac{\pi}{2}$
4	$\varphi_4 + \frac{\pi}{2}$	0	0	$\frac{\pi}{2}$
5	$\varphi_5 + \frac{\pi}{2}$	0	0	$\frac{\pi}{2}$
6	$\varphi_6 + \frac{\pi}{2}$	$-l_{\text{shank}}$	0	$\frac{\pi}{2}$
7	$\varphi_7 + \frac{\pi}{2}$	0	0	$\frac{\pi}{2}$
8	$\varphi_8 + \frac{\pi}{2}$	0	0	$\frac{\pi}{2}$
9	$\varphi_9 + \frac{\pi}{2}$	$-h_{\text{foot}}$	$l_{\text{toe_ankle}}$	0
10	0	0	$-l_{\text{foot}}$	0

Table 3: DH parameters for the lower limbs

The developed model allowed the analysis to begin from predefined joint angle configurations. Through direct kinematics, it provided critical data, including the position and orientation of the pelvis, right foot, and left foot. These outputs formed one of the two key inputs for the optimization process, as shown in Figure 22.

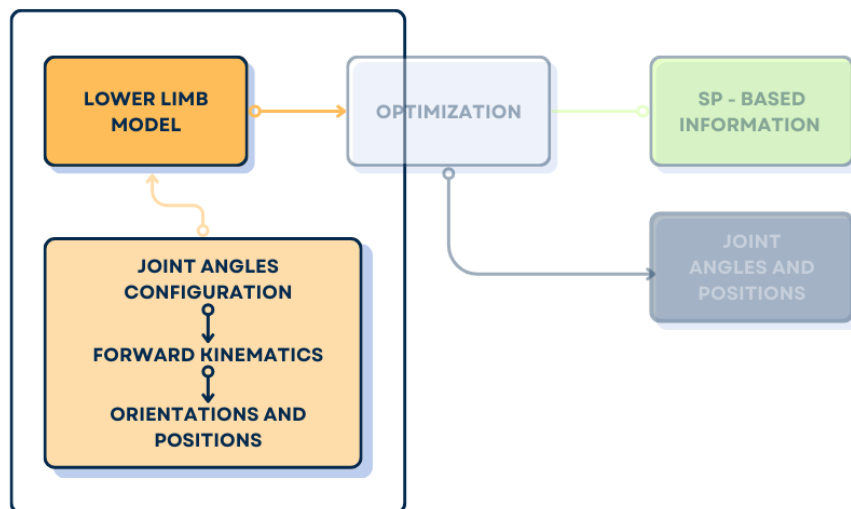


Figure 22: Overview of the KINEMI model, explicitly detailing the quantities obtained from the lower limb model.

4.4 SP - based information

The second input block for the optimization comprises data obtained from SP, as illustrated in Figure 24. In accordance with the Davis protocol outlined in [16], markers were positioned on key anatomical landmarks to record kinematic data during walking trials. As detailed in the previous Section 3.4, the Vicon output data were organized into a MATLAB structure named “data.mat”.

This structure contains the following information, on which all the processing is based:

1. **Physical marker trajectories:** 3D coordinates (x, y, z) of markers placed directly on the subject’s anatomical landmarks (**metto un elenco, o un’immagine**).
2. **Virtual markers:** derived outputs provided by Vicon (PlugIn gait), including both 3D trajectories (x, y, z) and axis-angle representations. These markers represent internal joint behaviors that are calculated rather than directly measured [6].

Specifically, the virtual markers include:

- **PEL:** represents the pelvis.
 - **RFE** and **LFE:** correspond to the right and left femoral ends, located at the knee joint center.
 - **RTI** and **LTI:** represent the right and left tibial ends, positioned at the ankle joint center.
 - **RTO** and **LTO:** represent the right and left toes, capturing the distal end of the foot.
 - **RFO** and **LFO:** represent the right and left forefoot markers, positioned on the dorsum of the foot closer to the ankle.
3. **Joint centers:** calculated positions representing the center of rotation for each joint, respectively hip, knee and ankle joint centers, as shown in the Figure 23 below.

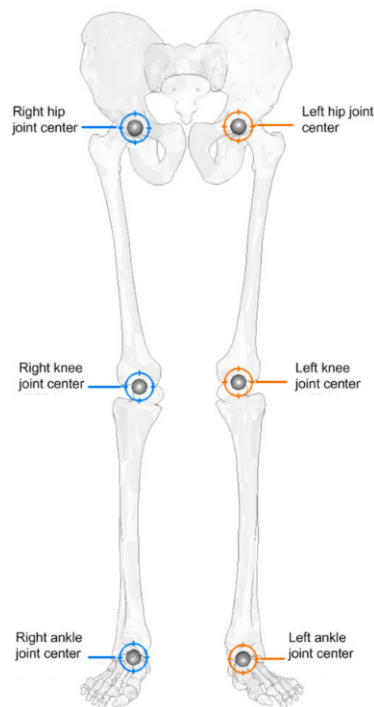


Figure 23: Representation of the lower limb skeletal structure with highlighted joint centers [6].

4. **Joint angles:** gold-standard outputs for hip, knee, and ankle angles, serving as a reference for the optimization process.

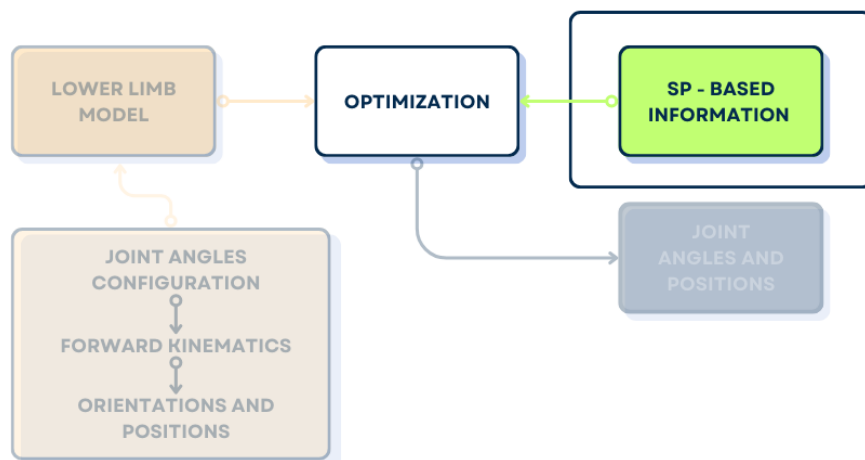


Figure 24: Overview of the KINEMI model, explicitly detailing the quantities obtained from the SP.

4.4.1 Data pre - processing

This section outlines the pre - processing steps undertaken to prepare kinematic data for the optimization. The initial focus is on computing rotation matrices to describe joint kinematics (*Step 1*), followed by aligning the data to the global reference system (*Step 2*), so to ensure consistency between local and global coordinate systems.

Step 1: computing Rotation Matrices

The initial step involves extracting angle-axis data for virtual markers from the dataset. This data is then converted into rotation matrices for all frames using a dedicated transformation process. By taking angle-axis data as input, this approach generates rotation matrices that describe the rotational behavior of key joints: hip, knee, and ankle. Specifically:

1. For each virtual marker, a rotation matrix for every frame in the dataset is computed. These markers correspond to the anatomical segments that define the proximal and distal components of the joints.

- The computed rotation matrices are organized into three structured variables: HIP, KNEE, and ANKLE. Each structure stores the matrices for the relevant proximal and distal segments of the joint. An example is depicted in Figure 25.

Once the rotation matrices have been calculated, they have been used to reconstruct the angles of interest of the joints (hip, knee, ankle), stored in the same structures. The values obtained can then be compared with those provided by the gold standard (Vicon output) as counter-evidence to validate the accuracy of the step.

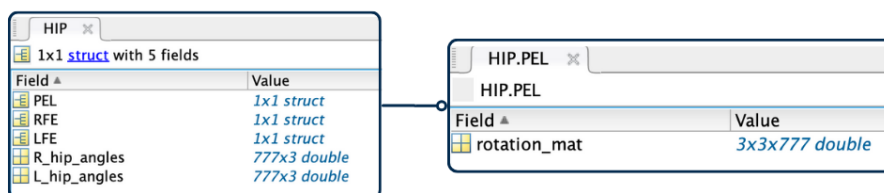


Figure 25: Example of the HIP structure in which both rotation matrices and joint angles are stored. The same applies to KNEE and ANKLE.

Step 2: Alignment

This step involves applying rotations to the kinematic data to prepare it for the optimization process.

As shown in Figure 26, the preliminary rotations applied here are used to transition from the **local reference system** of each body segment to the **base reference system**, in accordance with the definitions provided by the Vicon Plug-In Gait guide [6]. That said, each body segment (pelvis, femurs, tibias, and feet) has a local reference system, which is aligned to the base reference system using predefined rotation matrices.

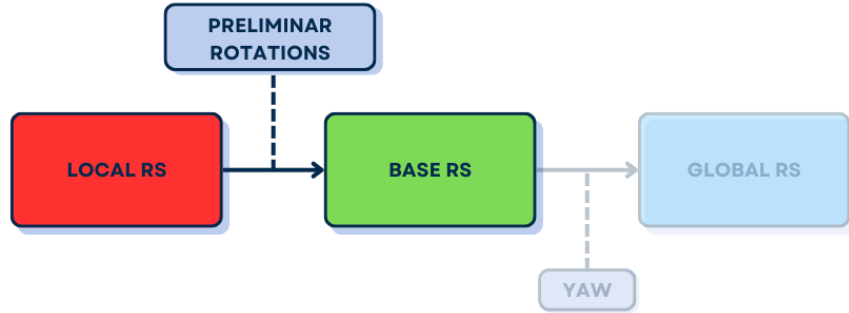


Figure 26: Overview of the first alignment step.

In the subsequent optimization process, an additional rotation equal to the **YAW** angle (rotation about the vertical Z-axis) is applied to transition from the base reference system to the Global Reference System (GRS), the one of the laboratory, as shown in Figure 27. This ensures that the data reflects the subject’s orientation in the laboratory space and aligns with the trajectory of motion as defined by the GRS. In fact, according to the Vicon Plug-In Gait guide [6]:

“The laboratory co-ordinate system is required here as a reference for the pelvis kinematics. The lab system is also used later in the definition of the foot co-ordinate frame. The global Z axis defines the vertical, i.e. perpendicular to the lab floor. The global X and Y axes are in the plane of the lab floor, with X often defining the direction of normal walking along the laboratory walkway.”

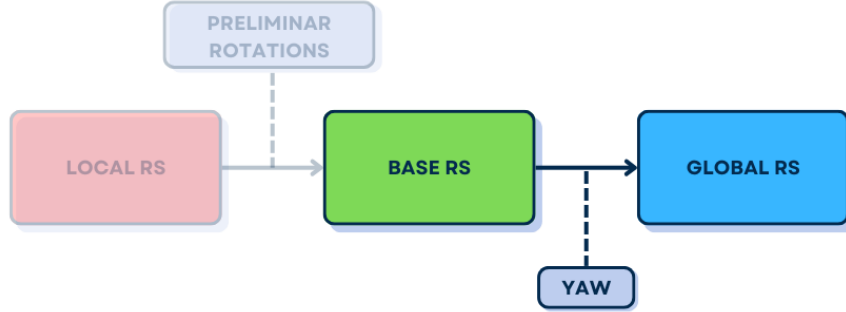


Figure 27: Overview of the second alignment step.

For each frame the following steps are executed:

1. **Data extraction:** the positions and rotation matrices of the pelvis, left and right femur, left and right tibia, and left and right feet are extracted. The positional data (p_P, p_LFE, p_RFE, etc.) is in millimeters and converted to meters by dividing by 1000. These data are then stored in arrays to manage all frames collectively.
2. **Rotation matrices definition**

Three predefined rotation matrices are established:

- R_x : a 90° rotation around x-axis, defined as

$$R_x = \begin{bmatrix} 1 & 0 & 0 \\ 0 & 0 & -1 \\ 0 & 1 & 0 \end{bmatrix} \quad (2)$$

- R_z : a -90° rotation around z-axis, defined as

$$R_z = \begin{bmatrix} 0 & 1 & 0 \\ -1 & 0 & 0 \\ 0 & 0 & 1 \end{bmatrix} \quad (3)$$

- R_y : a 90° rotation around y-axis, defined as

$$R_y = \begin{bmatrix} 0 & 0 & 1 \\ 0 & 1 & 0 \\ -1 & 0 & 0 \end{bmatrix} \quad (4)$$

3. Application of rotation

The extracted rotation matrices for each segment are adjusted to align the local reference system (red axes) with the base reference system (green axes), as shown in the explanatory example of Figure 28. The transformations are:

- **Pelvis:** a 90° rotation around the x-axis using R_x
- **Femurs** (left and right): a 90° rotation around the x-axis using R_x
- **Tibias** (left and right): a 90° rotation around the x-axis using R_x
- **Feet** (left and right): a compound rotation. First, a 90° rotation around the x-axis using R_x , followed by a -90° rotation around the z-axis using R_z

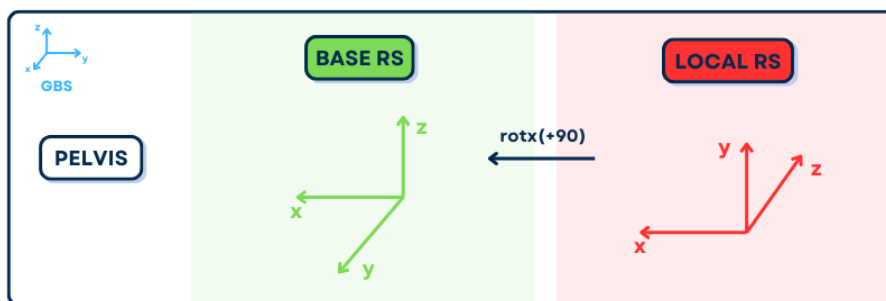


Figure 28: The rotation from the local SR of the pelvis into the corresponding base SR is shown here. The same is done for the femur, tibia and foot segments following the rotations explained above.

4.5 Optimization cycle

The optimization process is the core step. The primary goal is to satisfy the system's kinematic constraints while minimizing the error between measured and simulated data.

The following sub-chapter will discuss the main aspects of the optimization process, including:

- the Sequential Quadratic Programming (SQP) method,
- the formulation of the objective function,
- and the main outputs coming from the cycle.

4.5.1 The Sequential Quadratic Programming (SQP)

The optimization technique applied is based on the Sequential Quadratic Programming (SQP) algorithm, an iterative method designed for solving non-linear optimization problems with constraints. The SQP can be regarded as a quasi-Newton method and is particularly suitable for problems characterized by twofold continuously differentiable objective functions and constraints.

The SQP approach is based on the iterative solving of a series of quadratic programming (QP) subproblems, each of which minimizes a quadratic model of the objective while linearizing the constraints. The formulation of the QP subproblem is derived from a quadratic approximation of the Lagrange function, and its solution is used to define the new iteration, as summarized in Figure 29. Let us consider a non-linear programming problem in the form:

$$\begin{aligned} \min_{\mathbf{x}} f(\mathbf{x}) \\ \text{subject to: } \mathbf{h}(\mathbf{x}) \geq 0, \\ \mathbf{g}(\mathbf{x}) = 0. \end{aligned} \tag{5}$$

The Lagrange function associated with the problem is defined as:

$$L(\mathbf{x}, \boldsymbol{\lambda}, \boldsymbol{\sigma}) = f(\mathbf{x}) - \boldsymbol{\lambda}^\top \mathbf{h}(\mathbf{x}) - \boldsymbol{\sigma}^\top \mathbf{g}(\mathbf{x}) \tag{6}$$

where λ and σ represent the Lagrange multipliers associated with the unequal and equal constraints. In order to find a solution that satisfies the optimality conditions, an attempt is made to solve:

$$\nabla L(\mathbf{x}, \boldsymbol{\lambda}, \boldsymbol{\sigma}) = 0 \tag{7}$$

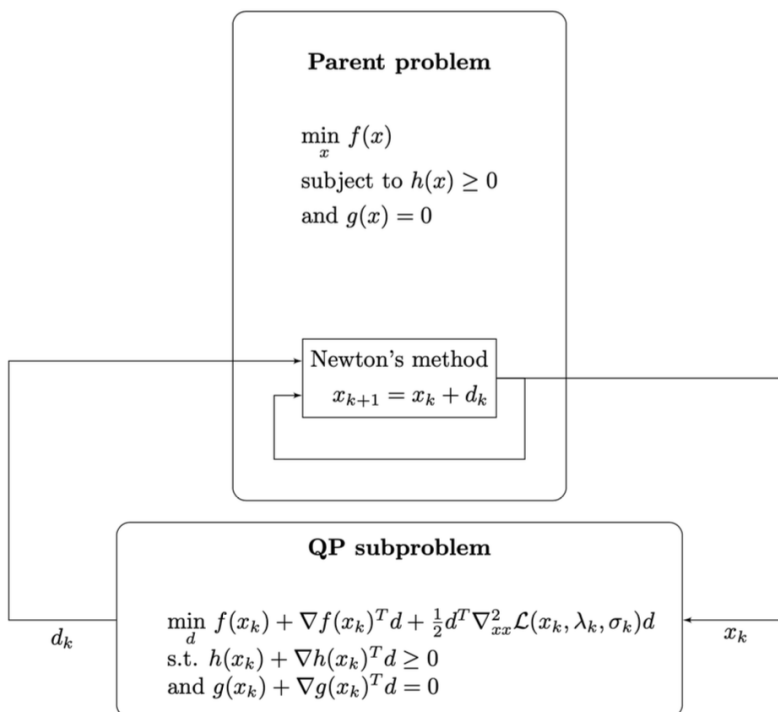


Figure 29: General schematic representation of the basic SQP algorithm [9]. The functions $f(x)$, $h(x)$, and $g(x)$ can be nonlinear, with x potentially representing a vector of multiple optimization variables. In this case, $h(x)$ and $g(x)$ correspond to systems of equations. The term ∇_{xx}^2 denotes the Hessian matrix.

The SQP algorithm calculates a search direction d_k at a current iteration $(x_k, \lambda_k, \sigma_k)$, solving a subproblem QP defined by:

$$\begin{aligned} \min_{\mathbf{d}} \quad & \frac{1}{2} \mathbf{d}^\top \mathbf{H}_k \mathbf{d} + \nabla f(\mathbf{x}_k)^\top \mathbf{d}, \\ \text{subject to:} \quad & \mathbf{h}(\mathbf{x}_k) + \nabla \mathbf{h}(\mathbf{x}_k)^\top \mathbf{d} \geq 0, \\ & \mathbf{g}(\mathbf{x}_k) + \nabla \mathbf{g}(\mathbf{x}_k)^\top \mathbf{d} = 0. \end{aligned} \tag{8}$$

where H_k is an approximation of the Hessian matrix of the Lagrange function.

The implementation of SQP consists of the following steps [18]:

1. Updating the Hessian matrix
2. Quadratic programming solution: to determine the search direction d_k

3. Initialization
4. Line search and merit function

4.5.2 Objective Function

The objective function is designed to minimize the error between the observed data and the model’s estimates, accounting for both the orientation and position of the body segments during walking. The minimization is based on the sum of the squares of the differences, a method that assigns larger penalties to more significant errors. The function consists of six terms, as shown in Figure 30.

$$f_{obj} = [R_{\Delta pelvis}, R_{\Delta RFoot}, R_{\Delta LFoot}, P_{\Delta pelvis}, P_{\Delta RFoot}, P_{\Delta LFoot}]$$

Figure 30: Objective function for the SQP algorithm.

Specifically:

- **Orientation:** orientation terms are evaluated by calculating the difference between the observed and model-estimated rotation matrix. This difference was converted to Euler Angles.

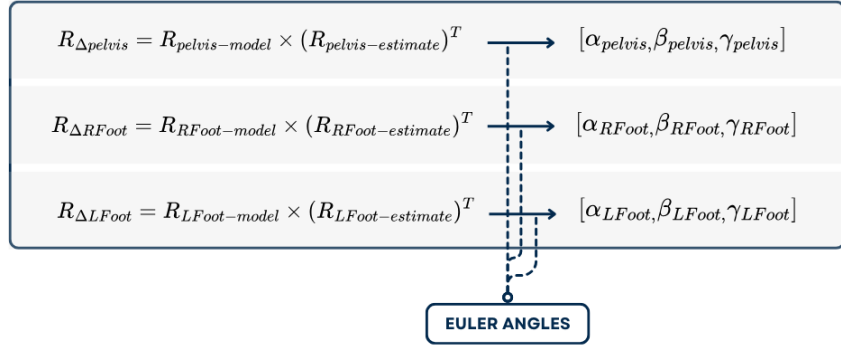


Figure 31: Computation of the difference between the observed rotation matrix and that estimated by the model, with subsequent conversion to Euler Angles. Note that the symbol “ \times ” denotes standard matrix multiplication, not the cross product.

- **Position:** position terms are calculated by comparing the observed coordinates with the estimated ones.

A distinctive aspect of the MATLAB implementation of the objective function, defined as `minimizeWalking_bis_v16_last` is its flexibility, enabled by the use of configurable parameters defined in `optionsCustom`, including:

- `usePelvisPos`, `usePelvisOri`
- `useThighsPos`, `useThighsOri`
- `useShanksPos`, `useShanksOri`
- `useFeetPos`, `useFeetOri`

These parameters function as Boolean flags (TRUE/FALSE) that can be set by the user to include or exclude specific error contributions, such as the orientation or position of various body segments. However, this flexibility was implemented actually to ensure the versatility and scalability of the code. In the specific configuration adopted in this thesis work, only the position and orientation contributions of the pelvis and feet were activated, as shown in Table 4 below.

Option	T/F
<code>usePelvisPos</code>	<code>true</code>
<code>usePelvisOri</code>	<code>true</code>
<code>useThighsPos</code>	<code>false</code>
<code>useThighsOri</code>	<code>false</code>
<code>useShanksPos</code>	<code>false</code>
<code>useShanksOri</code>	<code>false</code>
<code>useFeetPos</code>	<code>true</code>
<code>useFeetOri</code>	<code>true</code>

Table 4: Minimum input model.

The components of the objective function for both orientation and position are summed after being squared. This aggregation ensures that each difference contributes positively to the total error and penalizes larger discrepancies more significantly. The resulting function provides a single scalar value.

Figure 32 provides a summarized overview of the optimization process. The resulting outputs included joint angles and positions, allowing for the reconstruction of lower limb kinematics.

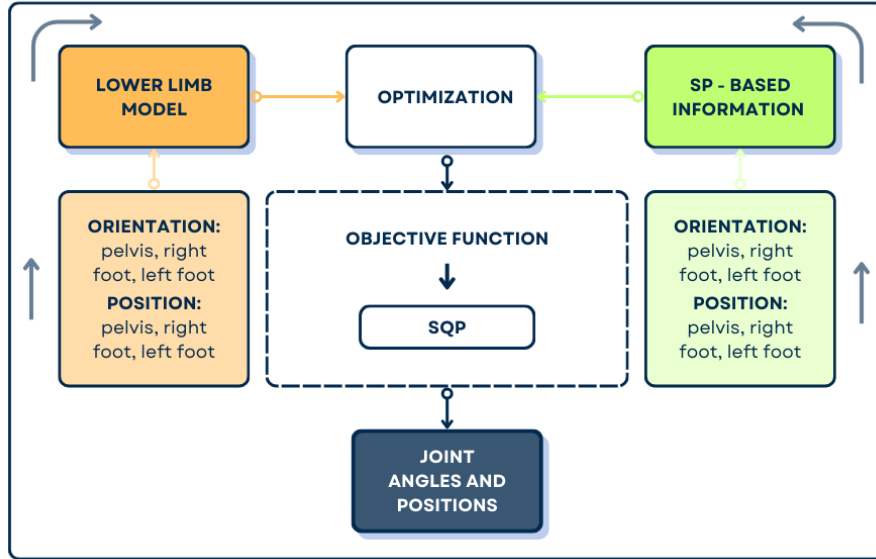


Figure 32: Optimization process made explicit

4.6 Joint Angles and positions

The developed KINEMI model was applied to both the datasets, generating joint angles and crucial positions as output. These outputs were essential for reconstructing lower limb kinematics.

4.7 Data analysis

4.7.1 Root Mean Square Error (RMSE) and Range of Motion (ROM)

Joint Angles and positions obtained were compared with those acquired from the SP to assess the accuracy of the estimation. To enable a quantitative assessment of the discrepancies between the results obtained through the KINEMI model and those recorded via the SP, Root Mean Square Error (RMSE) values were calculated. These values quantify the deviations between the two methods. The formula used for RMSE computation is presented below:

$$RMSE = \sqrt{\frac{1}{N} \sum_{i=1}^N (x_i - \hat{x}_i)^2} \quad (9)$$

where the terms x_i and \hat{x}_i represent the time-series data of angles obtained from the SP and the optimization framework systems, respectively. Removing the mean value from the two time series was not necessary because they both share the same reference system, as detailed above through the pre - processing steps. That said, the difference between the two series directly represents the error without the need for a correction.

Furthermore, the range of motion (ROM) is calculated by analyzing the entire time series and computing the ROM for each gait cycle. The final ROM is determined by taking the average of all ROM values associated with the individual gait cycles. The formula for the ROM for a single gait cycle is given by:

$$ROM = \max(x_i) - \min(x_i) \quad (10)$$

4.7.2 Statistical analysis

The aim of the statistical analysis was to explore the influence of different terrain conditions on the model results. To this end, a two-way ANOVA tests was used.

Terrain condition influence (Two-Way ANOVA)

This analysis was conducted to answer the question of whether the model provides comparable estimates of ROM across different terrain conditions and between the two measurement types (SP and Model). The goal is to determine whether terrain conditions significantly influence the ROM estimation or if the model maintains consistent performance regardless of the surface characteristics. The Two-Way Analysis of Variance (ANOVA) was applied to compare the Range of Motion (ROM) values directly, considering the measurement type and terrain condition as independent factors. The following factors were considered:

- **Factor 1:** measurement type (SP vs Model)
- **Factor 2:** terrain condition (cond01, cond02, etc.)

This test allows us to analyze:

1. The main effect of the measurement type (SP vs model)
2. The main effect of the terrain condition
3. The interaction effect between measurement type and terrain condition

The hypotheses for each factor and their interaction are defined as follows:

- Effect of measurements type (SP - model):
 - **Null hypothesis H_0** : there is no significant difference between ROM values obtained from SP and Model.
 - **Alternative hypothesis H_1** : there is a significant difference between ROM values obtained from SP and Model.
- Effect of terrain condition:
 - **Null hypothesis H_0** : different terrain conditions do not significantly influence ROM values.
 - **Alternative hypothesis H_1** : at least one terrain condition significantly influences ROM values.
- Interaction effect (measurement type \times terrain condition):
 - **Null hypothesis H_0** : there is no interaction between measurement type and terrain condition.
 - **Alternative hypothesis H_1** : the difference between SP and Model ROM values depends on the terrain condition.

The methodology involves:

1. **Normality assumption**: as explained in the previous paragraph for the One-Way ANOVA.
2. **Variance decomposition**

Here, the two-way ANOVA decomposes the total variance in the data into:

- **Variance due to measurement type**: how much the ROM estimates differ between SP and model.
- **Variance due to terrain condition**: how much ROM estimates vary across different conditions.
- **Variance due to interaction**: how the relationship between SP and Model varies depending on the condition.
- **Residual variance**: unexplained variation within each group. Residual variance represents the unexplained variability within each group after accounting for the effects of measurement type, terrain condition, and their interaction. It captures random noise, subject-specific differences, and other uncontrolled factors influencing ROM estimation.

3. Significance testing

For each factor and their interaction, the F-statistic is computed as shown in the formula 11 of the previous paragraph.

4. Decision rule

- If the **p-value** associated with the F-statistic is less than 0.05, H_0 is rejected, indicating a significant effect.
- If the **p-value** is greater than or equal to 0.05, H_0 cannot be rejected, suggesting the absence of significant differences.

5 Results

Figures 34–35 illustrate an example of the flexion-extension angles of the hip, knee, and ankle for both lower limbs over the entire time series. Figures 34 shows the results for the flat condition (right and left limb, respectively), while Figures 35 display the most irregular condition (Terrasensa). In each figure, the continuous blue line represents the angles estimated by the proposed model, while the dashed red line corresponds to the SP.

To quantitatively assess KINEMI model’s performance, RMSE values and ROM comparisons were computed, including absolute and percentage errors between the two methods. Section 5.1 presents RMSE results for the Turin dataset, where the model was developed, while Section 5.2 reports results for the Madrid dataset, used for testing and validation. Finally, Sections 5.3 and 5.4 detail the results of the statistical analysis.

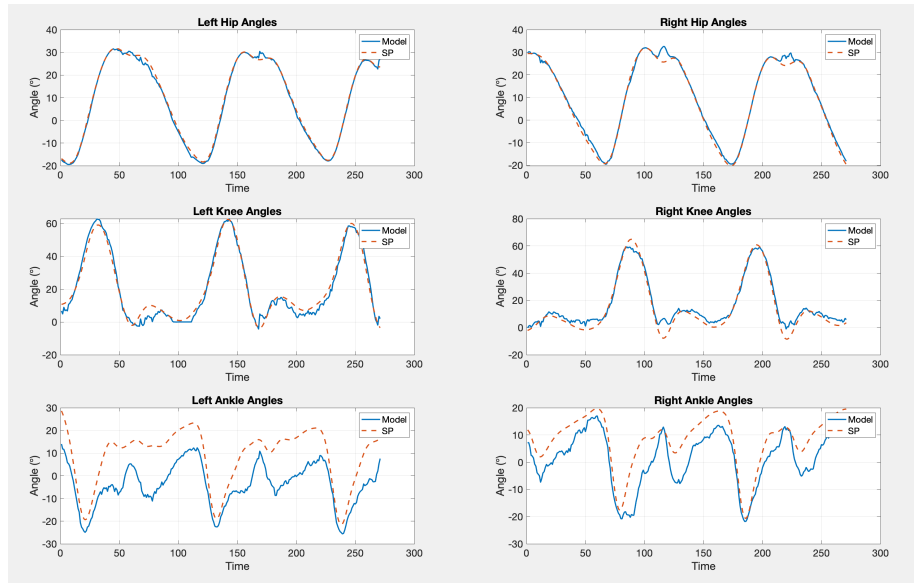


Figure 33: Left and right limb angles for hip, knee and ankle from the model (in blue) and SP (in red) - flat condition

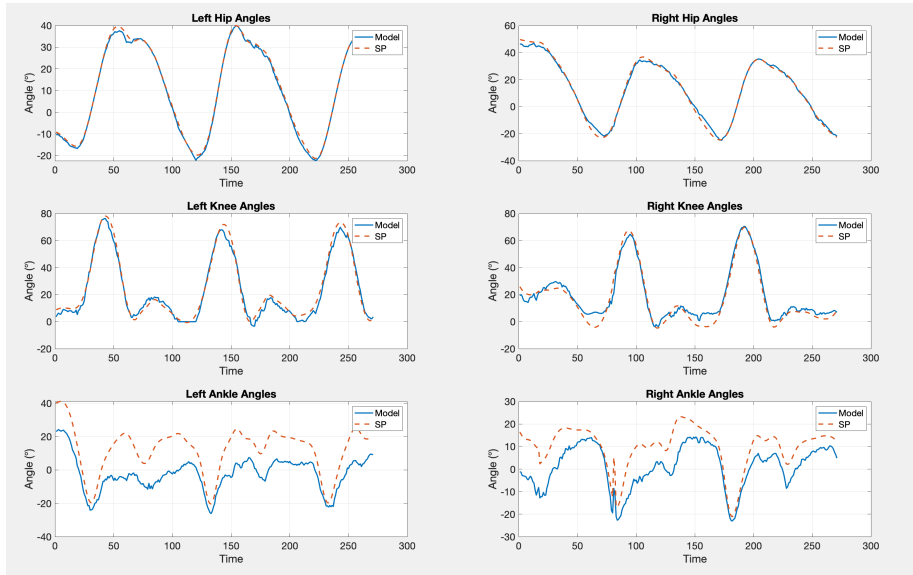


Figure 34: Left and right limb angles for hip, knee and ankle from the model (in blue) and SP (in red) - terrasensa condition

5.1 Dataset - Turin

RMSE results are presented in Table 5.

RMSE (deg)	RHip	LHip	RKnee	LKnee	RAnkle	LAnkle
dynamic01	1.1	2.3	2.7	2.3	2.4	2.3
dynamic02	1.6	2.3	3.5	5.4	3.2	3.3
dynamic03	1.5	2.7	2.4	5.4	2.7	3.7
dynamic04	1.4	2.3	3.6	5.0	3.0	2.7
dynamic05	1.9	1.6	3.3	3.6	1.7	3
dynamic06	1.6	2.1	3.8	5.2	2.9	3.3
dynamic07	2.8	1.9	5.0	4.2	3.2	3.5

Table 5: This table shows the RMSE values for each condition of walking (dynamic**), with values presented for each joint (RHip, RKnee, RAnkle, LHip, LKnee, LAnkle). The data include the mean RMSE values.

5.2 Dataset - Madrid

RMSE results are presented in Table 6 and Table 7. Table 8 and Table 9 present ROM results.

RMSE (deg)		RHip	LHip	RKnee	LKnee	RAnkle	LAnkle
Subj1	mean	1.9	1.5	4.7	3.8	9.6	15.6
	25th Perc	1.1	1.1	3.3	2.9	8.3	14.2
	75th Perc	2.5	1.5	5.4	3.9	10.1	16.7
Subj2	mean	1.2	1.1	7.0	5.0	3.4	7.4
	25th Perc	0.9	0.9	6.1	4.3	2.9	5.7
	75th Perc	1.3	1.3	8.0	5.5	4.0	9.0
Subj3	mean	2.6	1.8	10.3	4.6	6.0	2.0
	25th Perc	1.9	0.8	8.9	2.7	5.3	1.1
	75th Perc	2.9	1.8	11.0	4.1	6.1	1.9
Subj4	mean	1.5	2.1	3.0	4.9	5.3	2.9
	25th Perc	1.2	1.4	2.5	3.3	4.7	2.1
	75th Perc	1.6	2.1	3.5	4.8	5.5	3.1
Subj5	mean	1.2	1.1	5.3	5.3	7.6	9.5
	25th Perc	0.9	0.8	4.5	4.8	6.7	8.6
	75th Perc	1.4	1.2	6.2	6.0	7.9	10.3

Table 6: **Condition Averaging:** This table shows the RMSE values for each subject, with values presented for each joint (RHip, RKnee, RAnkle, LHip, LKnee, LAnkle). The data include the mean RMSE values, as well as the 25th and 75th percentiles for each joint across the subjects.

RMSE (deg)	RHip	LHip	RKnee	LKnee	RAnkle	LAnkle
Cond01	2.2	1.4	5.7	4.2	5.6	6.2
Cond02	1.7	2.7	5.9	7.1	6.9	8.8
Cond03	1.4	1.4	5.7	4.1	6.1	7.2
Cond04	1.9	1.5	6.8	4.9	6.6	7.7
Cond05	1.6	1.2	5.9	4.0	6.1	7.1
Cond06	1.5	1.1	6.2	4.0	6.4	7.7
Cond07	1.6	1.2	5.9	4.0	6.2	6.9
Cond08	1.6	1.7	6.3	5.4	7.0	8.2

Table 7: **(Subject Averaging)**: This table presents the RMSE values averaged across subjects for each condition. The values are organized by joint (RHip, RKnee, RAnkle, LHip, LKnee, LAnkle), showing the mean RMSE for each joint across the different conditions.

RIGHT LOWER LIMB									
ROM (deg)	RHip SP	RHip model	 SP MODEL 	RKnee SP	RKnee model	 SP MODEL 	RAnkle SP	RAnkle model	 SP MODEL
Cond01	42.9	44.9	2.0	56.3	53.5	2.8	32.0	29.8	2.1
Cond02	37.2	36.9	0.3	60.1	49.2	10.9	39.1	30.2	8.9
Cond03	45.4	46.0	0.6	60.7	56.2	4.5	32.4	27.8	4.6
Cond04	36.4	37.6	1.1	59.9	49.6	10.3	34.4	26.9	7.5
Cond05	53.4	54.5	1.1	76.7	71.0	5.5	32.7	27.7	5.0
Cond06	43.9	44.4	0.4	73.2	67.2	6.0	32.2	27.2	5.0
Cond07	48.9	48.7	0.3	63.4	60.1	3.4	30.0	24.8	5.3
Cond08	38.6	39.8	1.1	59.4	54.4	5.0	32.8	24.3	8.5

Table 8: This table presents the ROM values averaged across subjects for each condition, along with the observed absolute errors. The values are organized by joint (RHip, RKnee, RAnkle).

LEFT LOWER LIMB									
ROM (deg)	LHip SP	LHip model	SP MODEL	LKnee SP	LKnee model	SP MODEL	LAnkle SP	LAnkle model	SP MODEL
Cond01	46.0	45.1	1.0	58.0	58.4	0.7	32.5	27.4	5.1
Cond02	42.9	40.1	2.9	60.3	54.4	9.7	35.0	29.1	5.8
Cond03	47.1	45.5	1.6	63.2	59.8	5.4	34.2	26.3	7.9
Cond04	39.6	36.3	3.3	53.3	50.7	4.8	35.9	27.6	8.3
Cond05	57.9	56.2	1.8	75.9	72.1	5.0	33.6	29.2	4.4
Cond06	47.3	43.2	4.1	71.7	64.6	9.9	36.3	27.4	8.8
Cond07	48.9	49.5	0.7	63.5	61.5	3.1	29.1	24.8	4.2
Cond08	41.9	38.8	3.1	59.5	56.7	4.7	34.6	26.6	8.0

Table 9: This table presents the ROM values averaged across subjects for each condition, along with the observed absolute errors. The values are organized by joint (LHip, LKnee, LAnkle).

5.3 Effect of walking condition on model estimation

Factor	p-value
Type	$< 10^{-6}$
Condition	$< 10^{-16}$
Interaction	0.81

Table 10: This table presents p-values from the two-way ANOVA test for each factor considered.

6 Discussion

The aim of this study was to investigate lower limb kinematics using a minimal input configuration. Specifically, the proposed KINEMI model estimated angles at the hip, knee and ankle based on the position and orientation of the pelvis and feet. This approach was developed to overcome the limitations associated with traditional marker-based motion capture systems, seeking to provide an efficient and practical alternative for the study of gait. To validate KINEMI model, joint angles were reconstructed from experimental data collected in two datasets: one from the Turin laboratory, where the model was developed, and one from the Madrid laboratory, used for testing and validation. The reconstructed kinematics were compared with reference values obtained through a stereophotogrammetric system (SP), following the Plug-In Gait protocol. In this chapter, the results obtained from the proposed model are critically analyzed. The accuracy of the estimated joint kinematics is discussed in terms of RMSE and ROM errors. Additionally, the influence of different walking conditions on model performance is explored. Finally, the statistical analysis results are examined to determine whether significant differences exist between the proposed model and the SP system across different joints and conditions.

As shown in Figures 35-38, the hip, knee and ankle flexion-extension angles obtained from the proposed model are superimposed on those derived from the SP. The trends show the model's ability to effectively estimate joint motion. For illustrative purposes, the figures present the results for the simplest (flat) and the most irregular (terrasensa) conditions. It can be seen that the model is able to adequately estimate joint motion in both conditions, confirming its robustness even in the presence of terrain irregularities. There is a good match for hip and knee. However, a more pronounced discrepancy between the two estimates is evident for the ankle. This difference is attributable to the way in which Vicon's Plug-in Gait protocol defines the reference systems (SRs) for the tibial segment. Specifically, the protocol uses two separate SRs for the tibia, both defined in the ankle center (AJC):

- Untorsioned tibia, used for calculating knee angles
- Torsioned tibia, used for calculating ankle angles

Both of these reference systems share the same Z axis, but differ by a rotation around this axis due to the natural torsion of the tibia along its length. In the

model developed in this study, only one reference system could be defined for each body segment, and the untorsioned tibia was adopted for the tibia, as the main focus of the analysis was the kinematics of the knee. Moreover, we do not have access to the reference system of the torsioned tibia. The use of this SR also for the calculation of ankle angles introduces a systematic inaccuracy, as the natural rotation of the tibia is not correctly accounted for. This is reflected in the discrepancy observed in the trends of the ankle angles, which are less accurate than those of the hip and knee.

For a quantitative comparison between the trends obtained through optimization and those obtained through SP, aiming to quantify the errors incurred, the decision was made to calculate the errors between the two methodologies in terms of RMSE for each joint. The removal of the mean value as done in [19] was not necessary because the two systems share the same SR. The RMSE values are presented in two tables: Table 6 shows the mean per subject, telling when the model is accurate on average for each individual; Table 7 shows the mean per condition, telling when the model is accurate on average for each condition. The RMSE values show how the model appears to be more subject-dependent than condition-dependent, suggesting the importance of anthropometric measurements in the optimization process. This observation can be justified numerically by analyzing the ranges of RMSE values obtained in the two different averaging types:

- In condition averaging, the RMSE range across different conditions for a single subject is: RHip [1.2, 2.6] deg, LHip [1.1, 2.1] deg, RKnee [3.0, 10.3] deg, LKnee [3.8, 5.3] deg, RAnkle [3.4, 9.6] deg, LAnkle [2.0, 15.6] deg.
- In subject averaging, the RMSE range across different subjects for a single condition is: RHip [1.4, 2.2] deg, LHip [1.1, 2.7] deg, RKnee [5.7, 6.8] deg, LKnee [4.0, 7.1] deg, RAnkle [5.6, 7.0] deg, LAnkle [6.2, 8.8] deg.

It is evident that the RMSE ranges between subjects are generally wider than those between conditions, indicating that the model error depends more on individual characteristics than on variation in walking condition. This result is consistent with the hypothesis that anthropometric differences between subjects have a significant impact on the optimization process and the estimation of joint kinematics.

Beyond the RMSE assessment, the ROM values were computed for each joint. The computation of the ROM served as a basis for comparing the range

of values obtained between the two methods. The calculations were performed for both the optimization and SP cases, along with a comparison of the two methods, as presented in Tables 8-9.

A two-way ANOVA was performed to assess whether the model estimation was influenced by the experimental condition. A significant effect of 'Type' was found ($p = 0.0000$), indicating a difference between the SP and the model. A significant effect of 'Condition' was also observed ($p = 0.0000$), indicating that at least one condition differed from the others. No significant interaction between 'Type' and 'Condition' was detected ($p = 0.8064$), indicating that the difference between SP and the model was consistent across conditions.

7 Conclusions

Accurate quantification of kinematic parameters during real-life gait conditions is essential in human movement analysis. Their precise assessment can enhance diagnostic approaches for motor disorders and contribute to the development and evaluation of rehabilitation strategies. Although instrumental gait analysis provides highly accurate measurements, its clinical integration is hindered by logistical challenges. Emerging technologies, including wearable sensors and sensor fusion techniques, offer promising alternatives, enabling efficient gait monitoring in real-world environments.

This thesis addressed the impracticality of traditional methods in real-life conditions, investigating the feasibility, along with the associated limitations, of an approach based on a minimal sensor configuration strategically placed on the pelvis and feet.

The study employed a model called KINEMI based on the DH convention, introducing constraints to mitigate information gaps and errors. Validation against the SP demonstrated its effectiveness, with RMSE values highlighting the model's accuracy, particularly for hip and knee angles, while ankle estimates were affected by tibial torsion considerations. RMSE distributions also revealed that the model's accuracy was more subject-dependent than condition-dependent, underscoring the importance of anthropometric variability in the optimization process. The proposed framework complies with ISB standards, enabling its applicability in real-world settings and highlighting opportunities for further improvement.

This work confirmed the viability of a minimal sensor configuration for estimating gait kinematics, leveraging optimization techniques to mitigate measurement errors. Incorporating anthropometric variability enhanced estimation accuracy, although asymmetries and experimental uncertainties remain challenges. Given the objective of relying on fixed segment measurements, future work should focus on integrating segment length uncertainty into the optimization framework to improve robustness and support the broader application of IMU-based gait analysis.

Bibliography

- [1] F. Salis *et al.*, “A multi-sensor wearable system for the assessment of diseased gait in real-world conditions,” *Frontiers in Bioengineering and Biotechnology*, vol. 1, April 2023, (cit. on pp. i, 3, 18).
- [2] G. Wu *et al.*, “Isb recommendation on definitions of joint coordinate system of various joints for the reporting of human joint motion—part i: ankle, hip, and spine,” *Journal of Biomechanics*, vol. 35, Apr. 2002, (cit. on pp. 9, 10, 16).
- [3] E. S. Grood and W. J. Suntay, “A joint coordinate system for the clinical description of three-dimensional motions: Application to the knee,” *Journal of Biomechanical Engineering*, vol. 105, 1983, (cit. on pp. i, 1).
- [4] M. Wesseling, F. J. Vera-Garcia, E. J. Sánchez-Sánchez, R. Brunner, V. Camomilla, F. Cenni, J. A. Pons-Molina, S. Schmid, B. Vanwanseele, P. Wesseling, and J. Vanrenterghem, “Novel technologies for gait assessment in clinical practice: A systematic review,” *Applied Sciences*, vol. 11, 2021.
- [5] I. Meta Platforms, “Meta research,” <https://research.facebook.com/>.
- [6] V. M. Systems, *Vicon Plug-in Gait Reference Guide*, 2024, available as PDF on the official site.
- [7] S. F., “Analyzing human lower limb kinematics during walking: a challenging study with minimal inertial sensor configuration,” *Human Movement Science*, vol. 95, June 2024, relevant information is in the abstract.
- [8] B. Siciliano, L. Sciavicco, L. Villani, and G. Oriolo, *Robotics: Modelling, Planning and Control*. Springer London, 2009, (cit. on pp. 14, 15).
- [9] Wikipedia contributors, “Sequential quadratic programming,” *Wikipedia, The Free Encyclopedia*, pp. 23, 24, 2009, [Online; accessed 24-October-2023]. [Online]. Available: https://en.wikipedia.org/wiki/Sequential_quadratic_programming
- [10] S. Van Sint Jan, “Standardization of reporting of kinematic data,” *Gait Posture*, vol. 40, 2014.

- [11] W. Yin, W. Zhu, H. Gao, X. Niu, C. Shen, X. Fan, and C. Wang, “Gait analysis in the early stage of parkinson’s disease with a machine learning approach,” *Frontiers in Neurology*, vol. 15, p. 1472956, 2024, relevant information in the Introduction section.
- [12] A. A. Hulleck, D. Menoth Mohan, N. Abdallah, M. El Rich, and K. Khalaf, “Present and future of gait assessment in clinical practice: Towards the application of novel trends and technologies,” *Frontiers in Medical Technology*, vol. 4, December 2022, (cit. p 1).
- [13] S. Araki, H. Matsuura, T. Miyazaki, Y. Matsuzawa, Y. Nakai, M. Kawada, Y. Takeshita, M. Takamura, and R. Kiyama, “Longitudinal changes in vertical stride regularity, hip flexion, and knee flexion contribute to the alteration in gait speed during hospitalization for stroke,” *Human Movement Science*, vol. 95, June 2024, relevant information is in the abstract.
- [14] T. Huang, M. Ruan, S. Huang, L. Fan, and X. Wu, “Comparison of kinematics and joint moments calculations for lower limbs during gait using markerless and marker-based motion capture,” *Frontiers in Bioengineering and Biotechnology*, vol. 12, 2024.
- [15] K. Song, T. J. Hullfish, R. Scattone Silva, K. Grävare Silbernagel, and J. R. Baxter, “Markerless motion capture estimates of lower extremity kinematics and kinetics are comparable to marker-based across 8 movements,” *Journal of Biomechanics*, 2023.
- [16] R. B. Davis, S. Ounpuu, D. Tyburski, and J. R. Gage, “A gait analysis data collection and reduction technique,” *Human Movement Science*, 1991.
- [17] M. Caruso, L. Gastaldi, S. Pastorelli, A. Cereatti, and E. Digo, “An isb-consistent denavit-hartenberg model of the human upper limb for joint kinematics optimization: validation on synthetic and robot data during a typical rehabilitation gesture,” *2022 44th Annual International Conference of the IEEE Engineering in Medicine Biology Society (EMBC)*, pp. 1805–1808, 2022.
- [18] J. Nocedal and S. J. Wright, *Numerical Optimization*, 2nd ed. Springer, 2006, (cit. on p. 23).

- [19] P. Picerno, A. Cereatti, and A. Cappozzo, "Joint kinematics estimate using wearable inertial and magnetic sensing modules," *Gait Posture*, vol. 28, no. 4, pp. 588–595, Nov. 2008.